Electron g -factor of valley states in realistic silicon quantum dots

Ruskov, Rusko; Veldhorst, Menno; Dzurak, Andrew S.; Tahan, Charles

DOI
10.1103/PhysRevB.98.245424

Publication date
2018

Document Version
Final published version

Published in
Physical Review B

Electron *g*-factor of valley states in realistic silicon quantum dots

Rusko Ruskov,[1,*] Menno Veldhorst,[2] Andrew S. Dzurak,[3] and Charles Tahan[1,†]
[1]*Laboratory for Physical Sciences, 8050 Greenmead Dr., College Park, Maryland 20740, USA*
[2]*QuTech and Kavli Institute of Nanoscience, TU Delft, Lorentzweg 1, 2628CJ Delft, The Netherlands*
[3]*Centre for Quantum Computation and Communication Technology, School of Electrical Engineering and Telecommunications, The University of New South Wales, Sydney, NSW 2052, Australia*

(Received 20 October 2017; revised manuscript received 18 May 2018; published 27 December 2018)

We theoretically model the spin-orbit interaction in silicon quantum dot devices, relevant for quantum computation and spintronics. Our model is based on a modified effective mass approach which properly accounts for spin-valley boundary conditions, derived from the interface symmetry, and should have applicability for other heterostructures. We show how the valley-dependent interface-induced spin-orbit 2D (3D) interaction, under the presence of an electric field that is perpendicular to the interface, leads to a g-factor renormalization in the two lowest valley states of a silicon quantum dot. These g-factors can change with electric field in opposite direction when intervalley spin-flip tunneling is favored over intravalley processes, explaining recent experimental results. We show that the quantum dot level structure makes only negligible higher order effects to the g-factor. We calculate the g-factor as a function of the magnetic field direction, which is sensitive to the interface symmetry. We identify spin-qubit dephasing sweet spots at certain directions of the magnetic field, where the g-factor renormalization is zeroed: these include perpendicular to the interface magnetic field, and also in-plane directions, the latter being defined by the interface-induced spin-orbit constants. The g-factor dependence on electric field opens the possibility for fast all-electric manipulation of an encoded, few electron spin qubit, without the need of a nanomagnet or a nuclear spin-background. Our approach of an almost fully analytic theory allows for a deeper physical understanding of the importance of spin-orbit coupling to silicon spin qubits.

DOI: 10.1103/PhysRevB.98.245424

I. INTRODUCTION

Electronic g-factor arises as a direct consequence of the spin-orbit coupling (SOC); while relativistic in origin, SOC can be considerably modified in solids due to the electron's quasiparticle nature and a nontrivial band structure, as well as a result of heterostructure confinement effects (see, e.g., Ref. [1]). The variations of g-factor (and more generally, a SOC) in heterostructures and compounds in externally applied electric or magnetic fields is at the basis of spintronics and has led to a multitude of exotic proposals, ranging from spin transistors [2] to topological insulators [3]. While the SOC interaction is often considered in novel materials, it turns out to be a non-negligible effect in silicon as well [4]. As silicon is recognized as a promising material for spin-based quantum computing [5], understanding the manifiestation and influence of SOC in real devices takes on increased importance. Particularly relevant are lateral quantum dots (QD) realized in silicon heterostructures confining few electrons, which allow electric gate control of the spin system [6–18]. Silicon can be isotopically enriched to ^{28}Si and chemically purified (see, e.g., Ref. [19]), thus removing nuclear spin background as a major source of spin qubit dephasing. As a consequence of the increased qubit sensitivity to variations in resonance frequency, the g-factor's (weak) tunability with an applied electric field becomes an appreciable tool for qubit manipulation [10–13].

The standard description of the g-factor renormalization in a crystal is via a second-order perturbation theory (PT), using the bulk $\boldsymbol{k}\cdot\boldsymbol{p}$ Hamiltonian $\mathcal{H}(\boldsymbol{k})$ plus the spin-orbit interaction. It is given as a sum over the virtual electronic excited states (bands), where a relative contribution of an excited state depends on its coupling to the electron state of interest via the spin-orbit interaction Hamiltonian, and is suppressed by the corresponding energy denominator [20]. In Si, however, the bulk renormalization is very weak (of the order of $\delta g \sim 10^{-3}$), explained theoretically [20,21] by the large band-gap at the six equivalent conduction-band minima, at $\boldsymbol{k} \approx \hat{n} k_0$, (with $\hat{n} \equiv \pm\hat{x}, \pm\hat{y}, \pm\hat{z}$ and $k_0 \simeq 0.85\frac{2\pi}{a_0}$), Fig. 1(a). A presence of an external electric field $\boldsymbol{F}$ only weakly disturbs the crystal symmetry, which leads to even weaker effect for $\delta g(\boldsymbol{F})$ (to be discussed below). In a silicon heterostructure (in this paper, Si/SiO_2 is mainly considered as the confinement interface in the growth direction, however, the results are generally applicable to a Si/Ge heterostructures as well), the band structure is modified due to valley-orbit interaction, reflecting the reduction of the Si bulk crystal symmetry at the heterostructure interface. This generally leads to lifting of the sixfold degeneracy, e.g., for a heterostructure with a growth direction along [001], four of the valleys are lifted up in energy, while at crystal directions $\pm\hat{z}$ a superposition of the two valley states forms the lowest eigenvalley states,

*ruskovr@lps.umd.edu
†charlie@tahan.com

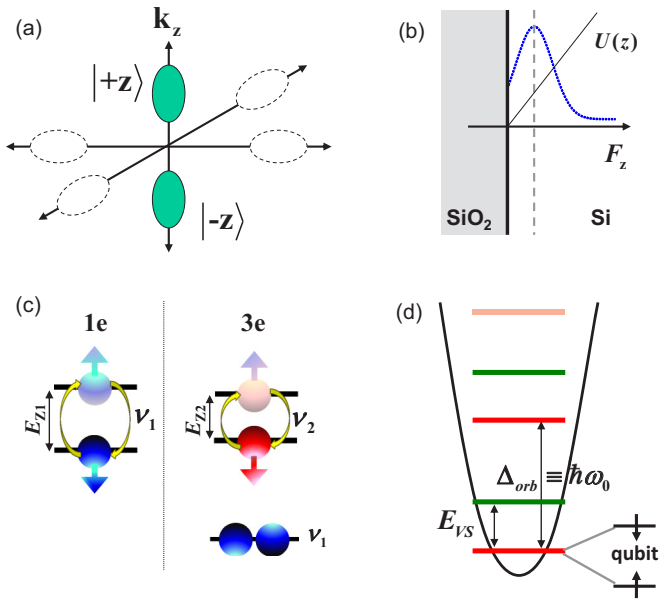

FIG. 1. (a) The six valleys in silicon. At a $(0, 0, 1)$ Si/SiO_2 interface (a MOS structure), the low-energy subbands are formed by the $\pm\hat{z}$ valleys. (b) Confinement in z direction at the Si/SiO_2 interface and with an applied electric field F_z, forms the eigenvalley states v_1, v_2, split by a tunable valley splitting $E_{VS} \propto F_z$, see Eq. (23). Note that the electron wave function $\varphi(z)$ and its derivative $\partial_z\varphi(z)$ may experience a discontinuity at the interface region [see Sec. II B and Eq. (8)]. [(c) and (d)] For a small quantum dot, the valley splitting is much smaller than the orbital splitting: $E_{VS} \ll \Delta_{orb} \equiv \hbar\omega_0$ (typically [7,11,16], $E_{VS} = 100$–500 μeV, $\Delta_{orb} = 2$–8 meV). (c) The one electron g-factor can be approximated by g_{v_1}, associated with the lower eigenvalley state v_1, while the three electron g-factor can be approximated by g_{v_2}, associated with the upper eigenvalley v_2. (d) Higher-orbital states only introduce a small second-order effect (Sec. IV B 2), such that one is actually measuring just the eigenvalley g-factors: $g_{1e} \simeq g_{v_1}$ and $g_{3e} \simeq g_{v_2}$.

which are split-off by the *valley splitting* E_{VS} [Figs. 1(a) and 1(d)]. An applied external electric field, $\boldsymbol{F} = (0, 0, F_z)$, enhances the valley splitting, varying in the range of few hundreds μeV, which was recently measured in Si quantum dot heterostructures [7,8] and confirmed by effective mass and tight-binding calculations [22–26].

It was stressed by Kiselev *et al.* [27,28] (see also Refs. [29–31]) that the g-factor renormalization can be equivalently represented as a first-order perturbation with the Hamiltonian $\delta\mathcal{H} = e\boldsymbol{A}\cdot\boldsymbol{V}_{\rm bulk}$, where $\boldsymbol{V}_{\rm bulk} = \hbar^{-1}\partial\mathcal{H}_{\rm bulk}(\boldsymbol{k})/\partial\boldsymbol{k}$ is the (bulk) velocity operator, and $\boldsymbol{A}(\boldsymbol{r})$ is the vector potential, which is a linear function of the radius vector $\boldsymbol{r}$ for a homogeneous magnetic field. In low-dimensional structures, such as a heterostructure or a quantum well (QW), this representation is argued to be more effective than the direct PT summation, leading to the expression for the g-factor tensor $(g_{\alpha\beta})$ [28,32]:

$$\tfrac{1}{2}\mu_B\sigma_{\alpha;ss'}g_{\alpha\beta}B_\beta \simeq \tfrac{1}{2}\mu_B\sigma_{\alpha;ss'}g_0B_\alpha + \langle e1, s|\delta\mathcal{H}|e1, s'\rangle, \quad (1)$$

where $s, s' = \pm 1/2$, σ_α are the Pauli matrices (for a 1/2-spinor), and $|e1, s\rangle$ are the Kramers-conjugate lowest subband states. Given, e.g., an in-plane magnetic field, the vector potential is $\boldsymbol{A} \sim z$, and the matrix element relates to the "bulk" g-factor renormalization as

$$\delta g_{\rm bulk} \propto \langle e1, s|\delta\mathcal{H}|e1, s'\rangle \propto \langle e1, s|zV_{\rm bulk}|e1, s'\rangle \simeq \langle z\rangle\mathcal{V}_{\rm bulk}. \quad (2)$$

The dependence of δg on an external electric field F_z (applied along the growth z direction, as is in the experiment) may arise from two distinct mechanisms: (i) from the z-confinement deformation of the $\langle z\rangle$ matrix element and (ii) from a more subtle mechanism, related to the energy dependence of the effective mass $m(E)$ and other parameters of the bulk $\boldsymbol{k}\cdot\boldsymbol{p}$ Hamiltonian (referred to as nonparabolicity effects: see, e.g., Ref. [33]).

The above, however, is not the whole story. In addition to the bulk $\boldsymbol{k}\cdot\boldsymbol{p}$ (effective mass) Hamiltonians $\mathcal{H}^{A,B}_{\rm bulk}(\boldsymbol{k})$ corresponding to the materials A, B that form the heterostructure, there is also an interface region (with size of the order of the materials' lattice constants, a_A, a_B). The latter can be described to a good approximation with an energy-independent transfer matrix $\hat{T}_{\rm if}$ that characterizes solely the interface region (see, e.g., Refs. [31,34–38]), and relates the wave functions and their derivatives, $\Psi^n_{A,B}$, $\partial_z\Psi^n_{A,B}$, at the interface [see Fig. 1(b) and the discussion below]; here, n enumerates the bands (and their degeneracies) in each material. The transfer matrix $\hat{T}_{\rm if}$ amounts to a certain boundary condition on the (envelope) wave function components $\Psi^n_{A,B}$, $\partial_z\Psi^n_{A,B}$, which can be equivalently expressed as an interface Hamiltonian $\mathcal{H}_{\rm if}(\boldsymbol{k})$. Thus one arrives at an "interface" g-factor renormalization of the form

$$\delta g_{\rm if} \propto \langle z\rangle\mathcal{V}_{\rm if}, \quad (3)$$

where $\mathcal{V}_{\rm if}$ is a "velocity" associated with the interface Hamiltonian [29,34,35,39]. We argue in what follows that in a Si/SiO_2-inversion layer the interface mechanism dominates the bulk, $\delta g_{\rm if} \gg \delta g_{\rm bulk}$. Physically, the interface contribution is expected to be large for quite distinctive materials such as Si/SiO_2; however, it cannot be excluded *a priori* in less distinctive heterostructures, e.g., in GaAs/AlGaAs or Si/Ge ones.

This paper is a thorough study of the theoretical construction and its consequences that was suggested in our original short paper publication [13]. Results include *general models of the valley splitting, valley-dependent SOC interactions, and valley-dependent anisotropic g-factors at a Si-heterostructure interface.* In particular, (1) we obtain an interface modified effective mass approach where the electron spin and valley components are mixed at the heterostructure interface via a nontrivial boundary condition (BC), in the presence of a perpendicular electric field, Sec. II. This BC is equivalent to intervalley tunneling plus intervalley and intravalley electron spin-flip processes, and reflects the interface C_{2v} symmetry. The derived interface Hamiltonian is singular (in the heterostructure growth z direction), which does not allow simple perturbation theory (PT) for the g-factor.

(2) We obtain from the BC a smooth interface 3D SOC tunneling Hamiltonian (Sec. III A) that allows PT for the g-factor renormalizations while maintaining the gauge invariance of the results. From the interface Hamiltonian, we derive the electric field dependent valley splitting at the Si heterostructure, Sec. III B, for a general interface-confinement potential, allowing us to interpret the experiment of Ref. [7].

(3) In the spin-valley mixing sector, we obtain, in a translationally invariant form, the valley-diagonal Rashba and Dresselhaus effective 2D SOC Hamiltonians, as well as the off-diagonal in eigenvalleys Rashba and Dresselhaus SOCs, Sec. III C. The corresponding valley-dependent Rashba and Dresselhaus SOC constants for a linear z confinement scale linearly with the electric field, $\propto F_z$, as does the valley splitting. The valley dependencies of the SOC constants suggest they may change sign when one switches between eigenvalleys, as a *consequence of the dominance of the intervalley spin-flipping processes versus the intravalley process*.

(4) The valley-dependent g-factor tensor renormalizations for an in-plane magnetic field are derived in Sec. IV B from the smooth interface 3D SOC Hamiltonians, scaling as $\propto F_z^{2/3}$ for a linear z confinement. For a perpendicular magnetic field, the relevant g-factor tensor components scale linearly with F_z, Sec. IV C, being proportional to the nonvanishing electric dipole matrix elements (cf. Refs. [7,40]).

(5) We show that the sign change of the SOC constants for different eigenvalleys leads to a corresponding sign change of the g-factor renormalization. In particular, for the in-plane magnetic field in a [110] direction, we derive qualitatively and quantitatively that the g-factor renormalization is opposite in sign for an electron occupying different eigenvalley states, Fig. 1(c), as it was observed in the experiment [13], Sec. IV B.

(6) A prediction is made for the g-factor angular dependence on the in-plane magnetic field, as well as for an out-of-plane magnetic field in Secs. IV B–IV D, that is in accordance with the C_{2v} interface symmetry, which was confirmed in current experiments [16,18]. The g-factor angular dependence provides a single QD spin qubit with decoherence sweet spots with respect to the magnetic field direction.

(7) In Secs. IV B and IV C, we consider second order corrections to the g-factor originating from the QD internal level structure, Fig. 1(d), also including the effect of interface roughness [7]. For both the in-plane and perpendicular magnetic field configurations, these corrections (for a Si QD with strong lateral confinement) can be neglected: $\delta^{(2)}g \sim 10^{-6}$.

(8) Finally, in Sec. IV E, we compare our results to various current experiments [13,16], providing in particular estimations for the ratio of the lower eigenvalley SOC constants, as well as for the difference of the SOC constants in both eigenvalleys subspaces with the account for the g-factor offsets for each eigenvalley. The dephasing mechanism introduced by the g-factor electric field dependence, is in a qualitative agreement with the experiment [13]. The results of Sec. IV can be seen as an experimental proposal to better understand the spin-valley structure at a Si interface. Section V contains the summary of results, and a discussion related to recent experiments with MOS QD structures [16]. More details of the derivations are presented in Appendices A–C.

II. Si/SiO$_2$ INTERFACE AND BOUNDARY CONDITIONS

A. Valley and spin scattering at a Si/SiO$_2$ heterostructure

We will consider a Si/SiO$_2$ heterostructure grown along the [001] ($\hat{z}$) direction with Si at $z > 0$ under an applied electric field in the $\hat{z}$ direction, $(0, 0, F_z)$ corresponding to a linear potential $U_z(z) = |e|F_z z$. Due to a large conduction band offset to SiO$_2$ ($\Delta_{\rm offset} \approx 3\,$eV), we will approximate it with an infinite boundary, $U_z(z) = \infty$, $z < 0$ [Fig. 1(b)].

A boundary condition at the heterostructure interface is a way to establish the interface scattering properties with respect to an incident wave [23,41] with a wave vector $\boldsymbol{k}$ close to the band minima. At the Si heterostructure, due to z confinement, there appear a mixing [42] between the two low-energy valley states [24,33,43,44] at $\boldsymbol{k}_0$ and $-\boldsymbol{k}_0$ [Figs. 1(a) and 1(b)], which implies intravalley or intervalley scattering. Generally, the scattering off the interface may lead not only to intervalley tunneling transitions ($\boldsymbol{k}_0 \to -\boldsymbol{k}_0$), but also to a spin flipping [25,31,33,43–45], $\sigma \to -\sigma$ (see below).

Assuming the generalized envelope functions [46], the total electron wave function is written in the single-band approximation as

$$\Psi(\boldsymbol{r}) = [\Phi_{\hat{z}}(\boldsymbol{r})\psi_{\boldsymbol{k}_0}(\boldsymbol{r}) + \Phi_{-\hat{z}}(\boldsymbol{r})\psi_{-\boldsymbol{k}_0}(\boldsymbol{r})], \tag{4}$$

where the Bloch functions at the two band minima (at the Δ points) are $\psi_{\pm\boldsymbol{k}_0}(\boldsymbol{r}) = e^{\pm i\boldsymbol{k}_0 z}u_{\pm\boldsymbol{k}_0}(\boldsymbol{r})$, and $u_{\pm\boldsymbol{k}_0}(\boldsymbol{r})$ are the periodic amplitudes. The $\Phi_{\pm\hat{z}}(\boldsymbol{r})$ are spinor envelopes corresponding to the two valleys: $\Phi_{\hat{z}}(\boldsymbol{r}) = [\Phi_{\hat{z},\uparrow}(\boldsymbol{r}), \Phi_{\hat{z},\downarrow}(\boldsymbol{r})]^T$ and $\Phi_{-\hat{z}}(\boldsymbol{r}) = [\Phi_{-\hat{z},\uparrow}(\boldsymbol{r}), \Phi_{-\hat{z},\downarrow}(\boldsymbol{r})]^T$, with spin components $\sigma = \uparrow, \downarrow$; the envelopes $\Phi_{\pm\hat{z}}(\boldsymbol{r}) = \Phi_{x,y}(x, y)\,\Phi_{\pm\hat{z}}(z)$ are separable in the absence of magnetic field.

In what follows, we consider an equivalent representation, in which the state is described as a four-component vector:

$$\Phi(\boldsymbol{r}) \equiv [\Phi_{\hat{z},\uparrow}(\boldsymbol{r}), \Phi_{\hat{z},\downarrow}(\boldsymbol{r}), \Phi_{-\hat{z},\uparrow}(\boldsymbol{r}), \Phi_{-\hat{z},\downarrow}(\boldsymbol{r})]^T, \tag{5}$$

subject to boundary conditions and tunneling Hamiltonians.

B. Boundary conditions for Si/SiO$_2$ heterostructure

The effective boundary condition at the Si/SiO$_2$-interface will act on the four-component envelope $\Phi(\boldsymbol{r})$, Eq. (5), and it is derived from symmetry reasonings, for an infinitely high barrier (assuming a left interface at $z = z_0^+ \equiv z_0 + \varepsilon$, $\varepsilon \to +0$):

$$\left(1 + iR\,k_z - R\,\frac{2m_l}{\hbar^2}\,V_{\rm if}(\boldsymbol{k})\right)\Phi(\boldsymbol{r})\,|_{z=z_0^+} \equiv \mathcal{B}\Phi(\boldsymbol{r})\,|_{z=z_0^+} = 0. \tag{6}$$

Here, $k_j \equiv -i\,\partial_j$ are quasimomentum operators ($j = x, y, z$), $\mathcal{B}$ is a boundary operator, R is a parameter of dimension of length, characterizing an abrupt interface [34,47], and it is assumed that $R \ll l_z, l_D$, where l_z, l_D are the QD confinement lengths along z direction and in lateral directions. For $R = 0$, Eq. (6) reduces to the standard BC, $\Phi(z)\,|_{z=z_0^+} = 0$ (which is unphysical, see Appendix C 3). For $R \neq 0$, the BC leads to spin and valley mixing at the interface via the 4×4 mixing matrix $V_{\rm if}(\boldsymbol{k})$ described in the next Sec. II C.

The form of the BC, Eq. (6), can be understood through the general transfer matrix formalism [36], where hermiticity of the Hamiltonian across the interface is preserved using a transfer matrix $\hat{T}$ (has to be Hermitian either) that relates the envelope function and its derivative normal to the interface on both sides of the interface (see also Refs. [31,37] for a recent account). For example, for the left interface for a single band and in the case of infinitely high barrier (spin-valley mixing is

dropped for a while):

$$0 = \begin{bmatrix} \Phi(z_0^-) \\ \partial_z \Phi(z_0^-) \end{bmatrix} = \begin{pmatrix} T_{11} & T_{12} \\ T_{21} & T_{22} \end{pmatrix} \begin{bmatrix} \Phi(z_0^+) \\ \partial_z \Phi(z_0^+) \end{bmatrix}, \tag{7}$$

and a nontrivial solution of (7) implies the "resonant condition"[48] $\det \hat{T} = 0$; so, $T_{12} \neq 0$. This means the relation

$$\Phi(z_0^+) + i R k_z \Phi(z_0^+) = 0, \tag{8}$$

reproducing the first two terms in (6) with $R \equiv T_{12}/T_{11}$, and implying a discontinuity of the wave function and its derivative at the interface: $\Phi(z_0^+) \neq 0$ and $k_z \Phi(z_0^+) \neq 0$. In the last form, using the dimensional interface parameter R, the BC was first derived in Ref. [34], by requiring preservation of the hermiticity of the Hamiltonian in the half-space, $z > z_0$. Physically, this implies continuity of the envelope flux density [31,34] (see also Appendix C 1). The parameter R, as well as the transfer matrix $\hat{T}$, is a characteristics of the interface boundary region; here, we will take it as a phenomenological parameter. An estimation, based on a two-band model (Appendix C 3) gives $|R| \approx 0.1 - 0.2$ nm in the case of a Si/SiO_2-interface.

If one drops the k_z term in Eq. (6), then the BC is of the usual "nonresonant type" (in the sense of Ref. [48]), with $T_{12} = 0$, and a transfer matrix obeys $\det \hat{T}_{\text{nonres}} \neq 0$; this implies a continuous envelop function at the interface [30]. Such BC have been suggested in Refs. [25,44,45] for the case of a Si/SiGe interface, and their "nonresonant" character make them different from ours, Eq. (6).

In this paper, we suggest that the surface contributions associated with the k_z term can be important. In particular, the interface contribution to the g-factor change will be zero without this term. We also note, that for $R > 0$, it is possible to consider the so-called Tamm states [49] (see also Refs. [31,34,47]), leading to localization in the $\hat{z}$ direction even in the absence of electric field (to be considered elsewhere).

C. The C_{2v} interface mixing matrix

The spin-valley mixing interface matrix $V_{\text{if}}(\boldsymbol{k})$ that enters the BC (6), can be expressed by taking into account the C_{2v} symmetry at the Si/SiO_2 interface (see, e.g., Refs. [1,25,44,45]).[1] The relevant C_{2v} invariants are the Rashba and Dresselhaus 2×2 forms: $H_R(\boldsymbol{k}) = \sigma_x k_y - \sigma_y k_x$, $H_D(\boldsymbol{k}) = \sigma_x k_x - \sigma_y k_y$. Indeed, for the C_{2v}-symmetry transformations [28,37], one gets (i) a π_z-rotation leading to $k_{x,y} \to -k_{x,y}$ and $\sigma_{x,y} \to -\sigma_{x,y}$, (ii) a reflection about the plane $(1, 1, 0)$, so that $k_x \leftrightarrow -k_y$ and $\sigma_x \leftrightarrow \sigma_y$, and (iii) a reflection about the plane $(1, \bar{1}, 0)$, with the $k_x \leftrightarrow k_y$ and $\sigma_x \leftrightarrow -\sigma_y$; it is then easy to see that $H_R(\boldsymbol{k})$ and $H_D(\boldsymbol{k})$ remain unchanged under these transformations. Thus, the 4×4 spin-valley mixing matrix is parameterized as

$$V_{\text{if}}(\boldsymbol{k}) = \begin{pmatrix} A(\boldsymbol{k}) & V\boldsymbol{I}_2 + B(\boldsymbol{k}) \\ V^*\boldsymbol{I}_2 + B^+(\boldsymbol{k}) & A(\boldsymbol{k}) \end{pmatrix}, \tag{9}$$

$$A(\boldsymbol{k}) \equiv s_D\, H_D(\boldsymbol{k}) + s_R\, H_R(\boldsymbol{k}), \tag{10}$$

$$B(\boldsymbol{k}) \equiv \chi_D\, H_D(\boldsymbol{k}) + \chi_R\, H_R(\boldsymbol{k}), \tag{11}$$

where $s_{D,R}$ are real parameters, while the intervalley tunneling matrix elements $V = |V| e^{i\phi_V(z_0)}$, and $\chi_{D,R} = |\chi_{D,R}| e^{i\phi_{D,R}(z_0)}$ generally possess phases [25,26,44]. For a general choice of the origin the phases depend linearly on z_0, $\phi_{V,D,R}(z_0) = \phi_{V,D,R} - 2ik_0 z_0$, as it follows from the original valley Bloch functions in Eq. (4). The 2×2 block-diagonal element $A(\boldsymbol{k})$ corresponds to *intravalley* spin-flipping transitions. The Rashba-type term $s_R(\sigma_x k_y - \sigma_y k_x)$ in the BC was previously derived [35,47] for single-valley semiconductors. The constant s_R has two contributions: $s_R = s_R^{\text{bulk}} + s_R^{\text{if}}$ and it can be shown that the bulk g^*-factor in Si can contribute to s_R^{bulk} (see, e.g., Refs. [29]). However, in this paper we argue that interface contributions are dominating. In particular, at the interface, both Rashba and Dresselhaus contributions will be allowed.

The off-diagonal elements $V\boldsymbol{I}_2$ and $B(\boldsymbol{k})$ are related to an *intervalley* tunneling (in momentum space). The non-spin-flipping term ($\sim V$) is responsible for the valley splitting [22,23,41] (see also Refs. [26,50,51] for recent account). The *intervalley* spin-flipping process will be described by the term $B(\boldsymbol{k})$. One of the main results of this paper is the observation that just this *intervalley* spin-flipping process is dominating the description of the experimentally measured g-factor variations [13].

D. Effective Hamiltonian for the Si/SiO_2 heterostructure

The effective two-valley Hamiltonian acts on the four-component vector $[\Phi_{\hat{z},\uparrow}(\boldsymbol{r}), \Phi_{\hat{z},\downarrow}(\boldsymbol{r}), \Phi_{-\hat{z},\uparrow}(\boldsymbol{r}), \Phi_{-\hat{z},\downarrow}(\boldsymbol{r})]^T \equiv \Phi(\boldsymbol{r})$, and includes a bulk Si (spin and valley degenerate) part

$$\mathcal{H}_0 = \left[\sum_{j=x,y,z} \frac{\hbar^2 k_j^2}{2m_j} + U_{x,y} + U_z \right] \times \boldsymbol{I}_4 \tag{12}$$

with the in-plane, $U_{x,y}$, and perpendicular to the interface, U_z, confinement electron potentials

$$U_{x,y} = \frac{m_t}{2}\left(\omega_x^2 x^2 + \omega_y^2 y^2\right), \tag{13}$$

$$U_z = \begin{cases} |e|(z - z_0)F_z, & z > z_0 \\ \infty, & z < z_0 \end{cases}. \tag{14}$$

In what follows, we consider a circular quantum dot [51], $\omega_x = \omega_y \equiv \omega_0$, and assume a much stronger confinement in the $\hat{z}$ direction: $l_z = (\hbar^2/2m_l|e|F_z)^{1/3} \ll l_D = (\hbar/m_t\omega_0)^{1/2}$, where m_l, m_t are the longitudinal and transverse effective masses for Δ-valley electrons, $|e|$ is the electron charge, and F_z is the z-confinement electric field. For the parameters of the experiment [7,11,13], for electric field $F_z \simeq 3 \times 10^7$ V/m, $l_z \approx 1$ nm. The lateral QD size is $l_D \approx 7$ nm for the 1e-case: $\Delta_{\text{orb}}^{1e} \equiv \hbar\omega_0 \simeq 8$ meV; for the 3e-case, $l_D \approx 14$ nm: $\Delta_{\text{orb}}^{3e} \simeq 2$ meV [since the "valence electron" in this case "sees"

[1]For ideal quantum well interfaces, the relevant interface symmetry (D_{2d} or D_{2h}) admits only the invariant structure corresponding to a Dresselhaus contribution [45], while with an applied perpendicular electric field the reduced C_{2v} symmetry admits also the Rashba structure.

Coulomb repulsion, Figs. 1(c) and 1(d)]. Here, $\Delta_{\rm orb}^{1e,3e}$, are the usual orbital splittings in the QD, Fig. 1(d).

The BC (6) induces a δ-functional Hamiltonian contribution, $\mathcal{H}_{\rm if}$ that mixes the spin and valley states:

$$\mathcal{H}_{\rm if} = -\frac{\hbar^2}{2Rm_l}\delta(z-z_0) \mp i\frac{\hbar^2}{2m_l}\delta(z-z_0)k_z + \delta(z-z_0)V_{\rm if}(\boldsymbol{k}). \tag{15}$$

[To show Eq. (15), one needs to integrate the Schrödinger equation with $\mathcal{H}_{\rm if}$ at the vicinity of the boundary, $z = z_0$.] The $-$ ($+$) sign at the second term in Eq. (15) stands for left (right) interface, with the replacement $z_0 = z_{\rm left}$ ($z_0 = z_{\rm right}$) and, in general, the interface parameters at the two interfaces may be different, $R_{\rm left} \neq R_{\rm right}$). For a strong enough electric field, the z confinement [Fig. 1(b)] will keep electrons close to the left interface ($l_z \ll d_{\rm QW} \equiv z_{\rm right} - z_{\rm left}$), and we will neglect the influence of the right interface.[2] We note that in the current experiment this is well fulfilled, since the ^{28}Si QW thickness is $d_{\rm QW} \approx 300$–800 nm, while $l_z \approx 1$ nm for $F_z \simeq 3\times 10^7$ V/m. Since $l_z \propto F_z^{-1/3}$, smaller electric fields are possible, providing the z-confinement energy splitting is much larger than the orbital splitting: $1.5\hbar^2/(m_l l_z^2) \gg \hbar^2/(m_t l_D^2)$; e.g., for $\Delta_{\rm orb} = 1$ meV one gets a typical field of $F_z \simeq 1.3\times 10^6$ V/m.

III. VALLEY SPLITTING, 2D(3D) EFFECTIVE HAMILTONIANS, AND INTERFACE SYMMETRY

A. The effective interface perturbation Hamiltonian

The interface contribution, Eq. (15), is essentially singular and cannot be used, in general, as a perturbation (except in a heuristic way). The effective interface perturbation Hamiltonian can be obtained by recasting the original problem of the Hamiltonian $\mathcal{H}_0$, Eq. (12), plus boundary conditions, Eq. (6), to a standard BC, $\mathcal{B}\Phi\,|_{z=z_0^+} \equiv \tilde{\Phi}\,|_{z=z_0^+} = 0$, and a transformed Hamiltonian. To this end, we consider the third term in the BC equation (6) as a perturbation (as $\langle k_x^2\rangle, \langle k_y^2\rangle \ll \langle k_z^2\rangle$) and replace the boundary operator $\mathcal{B}$ up to higher orders with a suitable unitary transform $\Gamma_{\rm BC}$ (Appendix A):

$$\tilde{\Phi}\,|_{z=z_0^+} \simeq \Gamma_{\rm BC}\Phi\,|_{z=z_0^+} = 0, \tag{16}$$

$$\tilde{\mathcal{H}} = \Gamma_{\rm BC}\mathcal{H}_0\Gamma_{\rm BC}^\dagger \simeq \mathcal{H}_0 + \delta\mathcal{H}, \tag{17}$$

with $\Gamma_{\rm BC} = 1 + i[Rk_z + R^2\frac{2m_l}{\hbar^2}V_{\rm if}(\boldsymbol{k})k_z]$. Keeping only the leading contribution in (17) of order $\mathcal{O}(R^2)$, one obtains

$$\delta\mathcal{H}(z) \simeq R\partial_z U_z + R^2\frac{2m_l}{\hbar^2}V_{\rm if}(\boldsymbol{k})\partial_z U_z. \tag{18}$$

In the following, we will neglect the first term in Eq. (18), which leads to a common energy shift only.

[2]Interference effects similar to that in Refs. [25,44] will be considered elsewhere

B. Approximate diagonalization of the interface matrix: Valley splitting

As suggested by the experiment [13], the valley splitting matrix element is much stronger than the corresponding spin matrix elements [52], $|V| \gg \{|\chi_{R,D}|, s_{R,D}\}\langle k_{x,y}\rangle$, and the interface spin-valley matrix is represented as $V_{\rm if}(\boldsymbol{k}) = V_{\rm if,val} + \mathcal{O}(1/|V|)$ with

$$V_{\rm if,val} = \begin{pmatrix} 0 & V\boldsymbol{I}_2 \\ V^*\boldsymbol{I}_2 & 0\end{pmatrix}. \tag{19}$$

Thus, one diagonalizes the interface Hamiltonian, Eq. (18), to leading order via the unitary transform (we choose below $z_0 = 0$ for convenience)

$$U_{\rm v} = \frac{1}{\sqrt{2}}\begin{pmatrix} \boldsymbol{I}_2 & -e^{i\phi_V}\boldsymbol{I}_2 \\ e^{-i\phi_V}\boldsymbol{I}_2 & \boldsymbol{I}_2\end{pmatrix}, \tag{20}$$

leading to the spin-independent valley-splitting Hamiltonian

$$\delta\mathcal{H}_{\rm if,val} = \frac{2m_l}{\hbar^2}R^2\,V_{\rm if,val}^{\rm d}\,\partial_z U_z, \tag{21}$$

with $V_{\rm if,val}^{\rm d} = {\rm diag}(|V|\boldsymbol{I}_2, -|V|\boldsymbol{I}_2)$. The corresponding spin-degenerate eigenstates are denoted as $|v_{2,\sigma}^{\rm d}\rangle = [C_\sigma^T, 0, 0]^T$ and $|v_{1,\sigma}^{\rm d}\rangle = [0, 0, C_\sigma^T]^T$ for the upper and lower eigenvalley states, respectively; C_σ is a spinor, corresponding to the two spin projections along an applied $\boldsymbol{B}$ field. Turning back to the original $\pm\hat{z}$-valley basis, the eigenstates of the leading-order Hamiltonian $\mathcal{H}_0 + \delta\mathcal{H}_{\rm if,val}$ will be written as

$$|\bar{v}_{i;\sigma}\rangle = \frac{1}{\sqrt{2}}\begin{bmatrix} C_\sigma \\ \mp e^{-i\phi_V}C_\sigma\end{bmatrix}\phi_0(x,y)\,\tilde{\varphi}_0(z), \quad i = 1,2, \tag{22}$$

where $\phi_0(x,y)\,\tilde{\varphi}_0(z)$ is an eigenstate of $\mathcal{H}_0$, Eq. (12), with BC, $\tilde{\varphi}_0(0^+) = 0$, in the lowest z subband. The upper/lower eigenvalley energies are $E_{2,1} = \langle\bar{v}_{2,1}|\delta\mathcal{H}_{\rm if,val}|\bar{v}_{2,1}\rangle = \pm\frac{|V|2m_lR^2}{\hbar^2}\langle\tilde{\varphi}_0(z)|\partial_z U_z|\tilde{\varphi}_0(z)\rangle \equiv \pm\frac{|V|2m_lR^2}{\hbar^2}\langle\partial_z U_z\rangle$ and the valley splitting reads

$$E_{\rm VS} = 2|V|R^2\frac{2m_l}{\hbar^2}\langle\tilde{\varphi}_0(z)|\partial_z U_z|\tilde{\varphi}_0(z)\rangle. \tag{23}$$

By observing the general integral relation (Appendix B 4)

$$\langle\tilde{\varphi}(z)|\partial_z U_z|\tilde{\varphi}(z)\rangle \equiv \int_0^\infty dz\tilde{\varphi}^*(z)\partial_z U_z\tilde{\varphi}(z) = \frac{\hbar^2}{2m_l}|\tilde{\varphi}'(0)|^2 \tag{24}$$

[it holds for any eigenstate of the Hamiltonian (12) with a smooth (at $z > 0$) z-confinement potential U_z and zero BC, $\tilde{\varphi}(0) = 0$], one can recast the valley splitting to the form

$$E_{\rm VS} = 2|V|R^2\,|\tilde{\varphi}_0'(0)|^2. \tag{25}$$

Alternatively, the valley splitting can be derived in a different (heuristic) way, using the singular Hamiltonian (15). In this case, one would consider the first two terms in Eq. (15) as a leading order boundary condition, recasting them to the Volkov-Pinsker form [34]

$$[1 + R\partial_z]\varphi_0(0) = 0, \tag{26}$$

[cf. Eq. (6)]. Since R is small, one essentially has the BC $\varphi_0(R) = 0$, which corresponds to z shifting the origin by R. With $\varphi_0(z)$ being the eigenstate of the Hamiltonian (12)

$\mathcal{H}_0$ with the above BC (26) one considers the "perturbation" $\delta(z)\, V^{\rm d}_{\rm if,val}$ from Eq. (15), with the diagonal part of the interface matrix. This gives the valley splitting

$$E_{\rm VS} = 2|V||\varphi_0(0)|^2 \simeq 2|V|R^2|\varphi_0'(0)|^2 \simeq 2|V|R^2|\tilde{\varphi}_0'(0)|^2, \tag{27}$$

where we have used Eq. (26), and that $\tilde{\varphi}_0'(0) \simeq \varphi_0'(0)$ up to higher orders in R. The result, Eq. (27), for the valley splitting coincides with Eqs. (23) and (25), obtained via the effective Hamiltonian (18).

Notice that for $\mathcal{H}_0$, Eq. (12), with the linear z-confinement potential $U_z = |e|F_z z$ (the "triangular" potential) one has the lowest energy subband function $\tilde{\varphi}_0(z) = N_1\, l_z^{-1/2}\, {\rm Ai}(l_z^{-1} z - \tilde{E}_1)$ with a normalization $N_1 \simeq 1.4261$, and $-\tilde{E}_1 = -2.3381$ being the first zero of the Ai function. The z average is $\langle z\rangle \simeq 1.5587\, l_z = 1.5587\, (\hbar^2/2m_l|e|F_z)^{1/3}$, see Eq. (12). For the valley splitting, one gets then from Eq. (23),

$$E_{\rm VS} = 2|V|R^2\, \frac{2m_l|e|F_z}{\hbar^2} = 2|V|R^2 l_z^{-3}. \tag{28}$$

Thus the general relation (25) we have proven (Appendix B 4) is fulfilled here from the relation $\frac{d\tilde{\varphi}_0(z)}{dz} = N_1\, l_z^{-3/2}\, {\rm Ai}'(l_z^{-1} z - \tilde{E}_1)$ and by noticing that $N_1 {\rm Ai}'(-\tilde{E}_1) = 1$.

For the second (heuristic) approach, with the "shifted BC" equation (26), the eigenstates of the Hamiltonian (12) will be just the shifted functions, with the lowest subband being

$$\varphi_0(z) = N_1\, l_z^{-1/2}\, {\rm Ai}\big(l_z^{-1}(z-R) - \tilde{E}_1\big), \tag{29}$$

and $|\varphi_0(0)| = R|\varphi_0'(0)| \simeq R|\tilde{\varphi}_0'(0)| \neq 0$, as implied by Eq. (25) and the Volkov-Pinsker BC, Eq. (26).

The linear dependence on F_z, Eq. (28), is confirmed experimentally [7,11]. Using the estimation $R \approx 0.1$ nm (Appendix C 3) and the experimental slope [7] $\frac{\Delta E_{\rm VS}}{\Delta F_z} = 1.32$ e Å, one gets a valley-splitting parameter $|V| \approx 2640$ meV Å compatible with the effective mass and tight-binding calculations [24,25] (extrapolated to the Si/SiO_2 case [53]).

Equation (28) corresponds to a valley splitting with linear F_z dependence and no offset, applicable for relatively large electric fields, $F_z \gtrsim 3\times 10^7$V/m, when z confinement is much stronger than lateral confinement. (Notice, however, that for larger QDs our results are applicable at lower electric fields as well.) On the other hand, the measurements of the valley splitting in our previous work [7,11] suggest that such offset could be possible. For example, a possible nonlinear dependence at small electric field suggested by tight-binding calculations [25,43] could lead to an effective offset.

Here, we propose a phenomenological approach that allows to describe the experimentally observed valley splitting offset [7,11] resulting from an interface localized interaction. Using the general results, Eqs. (23)–(27), one considers a confinement potential of the form $U_z = \frac{1}{2} m_l \omega_z^2 z^2 + |e|zF_z$, which provides a nonzero valley splitting at $F_z = 0$, with a confinement length factor, $l_{\rm osc}^{-3} \equiv |\tilde{\varphi}_0'(0)|^2 = \frac{8}{\sqrt{\pi}}(\frac{m_l\omega_z}{\hbar})^{3/2}$. In the opposite limit of large F_z, the zero-field confinement can be considered as a perturbation to the linear potential, leading asymptotically to the behavior $E_{\rm VS}^{\rm asympt} \simeq 2|V|R^2\, \frac{2m_l}{\hbar^2}(|e|F_z + m_l\omega_z^2\langle z\rangle)$, which can be interpreted as a positive offset. To obtain a negative offset, one needs to replace the interface-localized confinement with a repulsion z potential.

C. Approximate diagonalization of the interface matrix: the 2D Spin-Orbit Dresselhaus and Rashba couplings and effective 2D (3D) Hamiltonians

The effective spin-orbit Hamiltonians (of Rashba and Dresselhaus type) are obtained similarly to the $E_{\rm VS}$ calculation. For this end, we apply now the unitary transformation $U_{\rm v}$, Eq. (20), to the full interface matrix $V^{\rm U}_{\rm if}(\boldsymbol{k}) = U_{\rm v}^{+} V_{\rm if}(\boldsymbol{k}) U_{\rm v}$, and obtain the form

$$\begin{aligned} V^{\rm U}_{\rm if}(\boldsymbol{k}) &= \begin{pmatrix} |V|\boldsymbol{I}_2 & 0 \\ 0 & -|V|\boldsymbol{I}_2 \end{pmatrix} \\ &\quad + \begin{pmatrix} A + \frac{1}{2}B_{\rm diag} & \frac{1}{2}B_{\rm off} \\ {\rm H.c.} & A - \frac{1}{2}B_{\rm diag} \end{pmatrix} \\ &\equiv V^{\rm d}_{\rm if,val} + V^{\rm s\text{-}v}_{\rm if}(\boldsymbol{k}), \end{aligned} \tag{30}$$

with

$$B_{\rm diag} \equiv B(\boldsymbol{k}) e^{-i\phi_V(z_0)} + B^{+}(\boldsymbol{k}) e^{i\phi_V(z_0)}, \tag{31}$$

$$B_{\rm off} \equiv B(\boldsymbol{k}) - B^{+}(\boldsymbol{k}) e^{2i\phi_V(z_0)}, \tag{32}$$

obtained via Eq. (11), with $\phi_V(z_0) = \phi_V - 2ik_0 z_0$.

The spin-valley mixing part in (30), $V^{\rm s\text{-}v}_{\rm if}(\boldsymbol{k})$, consists of the (eigen)valley block-diagonal and off-diagonal parts and constitutes the spin-orbit effective coupling at the interface, derived from Eq. (18):

$$\begin{aligned} \delta\mathcal{H}_{\rm s\text{-}v} &= R^2 \frac{2m_l}{\hbar^2}\, V^{\rm s\text{-}v}_{\rm if}(\boldsymbol{k})\, \partial_z U_z \\ &= V^{\rm s\text{-}v}_{\rm if}(\boldsymbol{k})\, R^2 |\varphi_0'(0)|^2 \frac{\partial_z U_z}{\langle \partial_z U_z\rangle}, \end{aligned} \tag{33}$$

with matrix elements between the eigenvalley states v_1, v_2, that are proportional to the Rashba and Dresselhaus invariant forms, $H_R(\boldsymbol{k})$, $H_D(\boldsymbol{k})$. The spin-valley mixing Hamiltonian $\delta\mathcal{H}_{\rm s\text{-}v}$, Eq. (33), then reads

$$\begin{aligned} \delta\mathcal{H}_{\rm s\text{-}v} &= \begin{pmatrix} \alpha_{R;v_2} H_R + \beta_{D;v_2} H_D, & \alpha_{R;21} H_R + \beta_{D;21} H_D \\ \alpha^*_{R;21} H_R + \beta^*_{D;21} H_D, & \alpha_{R;v_1} H_R + \beta_{D;v_1} H_D \end{pmatrix} \\ &\quad \times \frac{\partial_z U_z}{\langle \partial_z U_z\rangle}, \end{aligned} \tag{34}$$

where $\alpha_{R;v_i}$, $\beta_{D;v_i}$, and $\alpha_{R;21}$, $\beta_{D;21}$ are the diagonal and off-diagonal (valley dependent) Rashba and Dresselhaus coupling constants, related to the effective SOC interactions considered below. We derive the SOC constants, taking into account the phases of $\chi_R = |\chi_R| e^{i\phi_R(z_0)}$, $\chi_D = |\chi_D| e^{i\phi_D(z_0)}$ in a translationally invariant form [54]. For the diagonal constants, one obtains

$$\alpha_{R;v_i} = [s_R \mp |\chi_R| \cos(\phi_R - \phi_V)]\, R^2 |\varphi_0'(0)|^2, \tag{35}$$

$$\beta_{D;v_i} = [s_D \mp |\chi_D| \cos(\phi_D - \phi_V)]\, R^2 |\varphi_0'(0)|^2, \quad i = 1,2 \tag{36}$$

with $-$ $(+)$ corresponding to the lower eigenvalley v_1 (upper eigenvalley v_2), respectively; this is similar to the relevant

strong field limit results of Ref. [25]. The off-diagonal Rashba and Dresselhaus coupling constants are, correspondingly,

$$\alpha_{R;21} = ie^{i\phi_V}|\chi_R|\sin(\phi_R-\phi_V)\,R^2|\varphi_0'(0)|^2, \quad (37)$$

$$\beta_{D;21} = ie^{i\phi_V}|\chi_D|\sin(\phi_D-\phi_V)\,R^2|\varphi_0'(0)|^2. \quad (38)$$

Notice that for a linear z confinement, Eq. (14), the SOC constants scale linearly with the applied electric field F_z. The off-diagonal elements $\alpha_{R;21}$, $\beta_{D;21}$ could be, generally, of the same order as the diagonal one, $\alpha_{R;v_i}$, $\beta_{D;v_i}$, depending on the phases, ϕ_V, ϕ_R, ϕ_D, and assuming $|\chi_{R,D}| \gtrsim s_{R,D}$. These parameters, including the phases, enter in the observable SOC constants in certain combinations, relating the diagonal to off-diagonal (in valley) SOC constants, Eqs. (35)–(38). Equations (34) and (35)–(38) describe the 3D spin-valley mixing at the interface. These equations are one of the main results of this paper, together with the g-factor derivation in the next chapter, which will be based on them as well.

A 2D version can be obtained by integration over the z direction. The effective 2D Hamiltonian with Rashba and Dresselhaus contributions in each eigenvalley subspace is given by the corresponding block-diagonal parts in Eq. (34):

$$\mathcal{H}^{\rm 2D}_{v_i} = \alpha_{R;v_i}\,H_R(\boldsymbol{k}) + \beta_{D;v_i}\,H_D(\boldsymbol{k}), \quad i=1,2, \quad (39)$$

with the 2D spin-orbit couplings given by Eqs. (35) and (36). Similarly, the 2D Hamiltonian that describes the off-diagonal transitions between the eigenvalley subspaces v_1, v_2 can be written in the form

$$\mathcal{H}^{\rm 2D}_{v_2,v_1} = \alpha_{R;21}H_R(\boldsymbol{k}) + \beta_{D;21}H_D(\boldsymbol{k}), \quad (40)$$

with the 2D spin-orbit couplings given by Eqs. (37) and (38).

As seen from Eqs. (35)–(38), all the above spin-orbit constants depend on the common matrix elements constants, V, s_R, s_D, χ_R, and χ_D, that parametrize the spin-valley mixing boundary condition, Eq. (6). We note that the 2D spin-orbit Rashba and Dresselhaus constants, $\alpha_{R;v_i}$, $\beta_{D;v_i}$, may change sign when one switches between the eigenvalley subspaces $v_1 \to v_2$:

$$\alpha_{R;v_1} \simeq -\alpha_{R;v_2} \text{ and } \beta_{D;v_1} \simeq -\beta_{D;v_2} \quad (41)$$

if the intervalley contributions, χ_R, χ_D dominate the intravalley ones, s_R, s_D; Eq. (41) is exact for $s_R, s_D = 0$. As shown in the next Sec. IV, this is in qualitative agreement with the experiment [13], where measurements of the g-factor were performed for an in-plane magnetic field.

Finally, we mention that one can derive the 2D Hamiltonian (34) without recasting the BC to a smooth perturbation Hamiltonian [as it was done in Eqs. (17) and (18)]. As in the valley splitting derivation in Eq. (27), one just refers to the leading order BC, Eq. (26), and uses (heuristically) the singular "perturbation" $\delta(z)\,V^{\rm U}_{\rm if}(\boldsymbol{k})$ with the full interface matrix, Eq. (30). The effective interface Hamiltonian, Eq. (18), is necessary, however, for the derivation of the g-factor where the heuristic approach does not work.

IV. ELECTRON g-FACTOR AT THE INTERFACE

A. Derivation of the g-factor corrections

We will consider for each eigenvalley the Hamiltonians, Eqs. (12) and (21), $\widetilde{\mathcal{H}}_0 = \mathcal{H}_0 + \delta\mathcal{H}_{\rm if,val}$ as the zeroth-order term, and the spin-valley mixing term $\delta\mathcal{H}_{\rm s\text{-}v}$, Eqs. (33) and (34), as a perturbation. Since the valley splitting is large, one can neglect the block-off-diagonal part in $\delta\mathcal{H}_{\rm s\text{-}v}$ as it contributes to the energy renormalization of the subspaces v_1, v_2, only in second order of PT, and is suppressed as $\sim|\chi_{D,R}\langle k_{x,y}\rangle|/E_{\rm VS}$. The block-diagonal parts of $\delta\mathcal{H}_{\rm s\text{-}v}$ are of the form

$$\mathcal{H}^{\rm 3D}_{v_i} = [\alpha_{R;v_i}\,H_R(\boldsymbol{k}) + \beta_{D;v_i}\,H_D(\boldsymbol{k})]\,\frac{\partial_z U_z}{\langle\partial_z U_z\rangle}, \; i=1,2. \quad (42)$$

One can note that these Hamiltonians are in one-to-one correspondence, via Eqs. (17) and (18), to the BCs in each eigenvalley subspace [55]:

$$\left\{1 + iRk_z - R\frac{2m_l}{\hbar^2}[\mp|V| + V_{v_i}(\boldsymbol{k})]\right\}\Phi_{v_i}(\boldsymbol{r})\,|_{z=z_0^+} = 0, \quad (43)$$

with the spin-mixing matrix $V_{v_i}(\boldsymbol{k}) \equiv A \mp \frac{1}{2}\,B_{\rm diag}$ defined in Eqs. (10), (11), and (31), and acting on the corresponding eigenvalley spinors, Φ_{v_i}, $i=1,2$. Equation (42) may contribute to first order of PT to the g-factor in each eigenvalley subspace.

For a magnetic field a direct Zeeman term is added to the zeroth-order Hamiltonian $\widetilde{\mathcal{H}}_0$:

$$\mathcal{H}_{\rm Z} = g^*\mu_B\tfrac{1}{2}\boldsymbol{\sigma}\boldsymbol{B}, \quad (44)$$

where $\mu_{\rm B}$ is the Bohr magneton; the bulk Si effective g^*-factor [20,21,56], is $g^*_{\rm Si} \simeq 1.9983$ (at the interface).

The perturbation due to external magnetic field will arise via the replacement [46] $k_j \to k_j + \frac{|e|}{\hbar}A_j(\boldsymbol{r})$ [$\boldsymbol{A}(\boldsymbol{r})$ is the vector-potential], both in $\mathcal{H}_0$ and in the interface Hamiltonian $\delta\mathcal{H}_{\rm s\text{-}v}$ or, equivalently, in the respective BCs, Eqs. (6), (15), and (43), which makes the problem gauge invariant [for a gauge-invariant BC without spin and valleys, see Appendix C 1; for a discussion of gauge-invariance see Appendix C 2]. Introducing the magnetic length, $l_B = (\hbar/|e|B)^{1/2}$, we require a stronger z confinement, $l_z \ll l_B$, which is fulfilled in the experiment for $B = 1.4$ T, as $l_B(1.4\text{ T}) \simeq 22$ nm.

B. g-factor for in-plane magnetic field, $B_\parallel$

1. $\delta g_\parallel$ to first-order PT

For an in-plane magnetic field, one chooses the gauge $\boldsymbol{A}_\parallel(\boldsymbol{r}) = (B_y z, -B_x z, 0)$. In what follows, we neglect small corrections originating from the bulk Hamiltonian $\mathcal{H}_0$, Eq. (12). The perturbation to Eq. (42), $\delta_B\mathcal{H}^{\rm 3D}_{v_i}$, due to nonzero magnetic field $\boldsymbol{B}_\parallel$, contributes to the g-factor interface contribution, $\delta g^{v_i}_\parallel$, to first order. Averaging Eq. (42) over the states $|\bar{v}_i\rangle \equiv |v_i\rangle \otimes |\phi_{v_i}(\boldsymbol{r})\rangle$ [that includes the envelope wave

function of the confined electron $|\phi_{v_i}(\boldsymbol{r})\rangle \equiv \phi_0^{v_i}(x,y)\varphi_0(z)$, see below], for each eigenvalley gives

$$\langle \bar{v}_i|\delta_B \mathcal{H}_{v_i}^{3D}|\bar{v}_i\rangle = a[U_z]\,\mu_B[\alpha_{R;v_i}(\sigma_x B_x + \sigma_y B_y) - \beta_{D;v_i}(\sigma_x B_y + \sigma_y B_x)], \quad i=1,2; \tag{45}$$

$$a[U_z] \equiv -\frac{|e|}{\hbar\mu_B}\frac{\langle z\partial_z U_z\rangle}{\langle \partial_z U_z\rangle}, \quad a[U_z]\sim 10^{-3}, \tag{46}$$

with the constant $a[U_z]$ being a weakly dependent functional of the z-confinement potential U_z. For a constant electric field $a[U_z]$ is replaced by $-\frac{|e|\langle z\rangle}{\hbar\mu_B}$. The total Zeeman energy can be written via the g-factor tensor:

$$\mathcal{H}_{Z,v_i}^{\rm tot} = \sum_{\alpha,\beta}\frac{1}{2}\mu_B\left(g_0\delta_{\alpha\beta} + \delta g_{\alpha\beta}^{v_i}\right)\sigma_\alpha B_\beta, \tag{47}$$

where $g_0 = g_{\rm Si}^*$ is the bulk value in Si, and

$$\delta g_{xx}^{v_i} = \delta g_{yy}^{v_i} = -a[U_z]\,\alpha_{R;v_i}, \tag{48}$$

$$\delta g_{xy}^{v_i} = \delta g_{yx}^{v_i} = +a[U_z]\,\beta_{D;v_i}. \tag{49}$$

The Zeeman splitting is expressed as $\Delta E \equiv \mu_B g_\parallel(\varphi)B_\parallel$, $B_\parallel = \sqrt{B_x^2+B_y^2}$, and $B_x = B_\parallel\cos\varphi$, $B_y = B_\parallel\sin\varphi$, being the magnetic field components along the Si crystal axes. By diagonalization of the Hamiltonian (47) for each valley subspace, one obtains the total g-factor $g_\parallel^{v_i}(\varphi, F_z)$,

$$g_\parallel^{v_i}(\varphi,F_z) = \Big(g_0^2 + 2a[U_z]\,g_0\,[\alpha_{R;v_i} - \beta_{D;v_i}\sin 2\varphi] + a[U_z]^2\left[\alpha_{R;v_i}^2 + \beta_{D;v_i}^2 - 2\alpha_{R;v_i}\beta_{D;v_i}\sin 2\varphi\right]\Big)^{1/2}, \tag{50}$$

which includes the interface contribution $\delta g_\parallel^{v_i}$: $g_\parallel^{v_i} \equiv g_0 + \delta g_\parallel^{v_i}$. The F_z dependence in Eq. (50) is implicit via the SOC constants and z averages, Eqs. (35), (36), (24), and (46). To first order in $a[U_z]$, it gives the g-factor interface variation as a function of the in-plane magnetic field direction [57,58], φ (Fig. 2):

$$\delta g_\parallel^{v_i}(\varphi,F_z) \simeq \delta^{(1)} g_{v_i} = -\frac{|e|}{\hbar\mu_B}\frac{\langle z\partial_z U_z\rangle}{\langle\partial_z U_z\rangle}(\alpha_{R;v_i} - \beta_{D;v_i}\sin 2\varphi). \tag{51}$$

The angular dependence on the direction of the in-plane magnetic field suggests that there could be valley-dependent "sweet spot directions" φ_{v_i} where the g-factor variation with the electric field is zero. Since from Eq. (51),

$$\frac{\partial[\delta g_\parallel^{v_i}(\varphi,F_z)]}{\partial F_z} = \frac{\partial \ln\langle z\,\partial_z U_z\rangle}{\partial F_z}\,\delta g_\parallel^{v_i}(\varphi,F_z), \tag{52}$$

the g-factor noise variation gets to zero together with $\delta g_\parallel^{v_i}(F_z)$. For a given eigenvalley v_i, the choice of the angle φ_{v_i} will depend on the size and sign of the Rashba and Dresselhaus 2D spin-orbit constants, $\alpha_{R;v_i}$, $\beta_{D;v_i}$. The first-order PT g-factor correction, Eq. (51), can be put to zero when $\sin(2\varphi) = \alpha_{R;v_i}/\beta_{D;v_i}$. Thus the optimal angles are expressed as (Fig. 2)

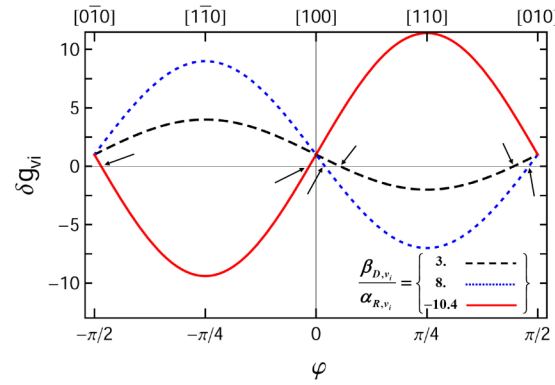

FIG. 2. Angular dependence of the g-factor correction $\delta g_\parallel^{v_i}(\varphi, F_z)$, Eq. (51), at different ratios of the spin-orbit parameters: $\beta_{D;v_i}/\alpha_{R;v_i} = \{3.0,\ 8.0,\ -10.4\}$ (dashed black, dotted blue, and red curves, respectively); $\delta g_\parallel^{v_i}$ is in units of $\frac{e}{\hbar\mu_B}|\alpha_{R;v_i}|$. For $\boldsymbol{B}_\parallel$ at angles (shown with arrows) φ_{v_i}, Eq. (53), measured from the [1, 0, 0] crystal direction, the QD spin-qubit is immune to the charge noise on F_z, since the g-factor variation due to electric field noise goes to zero together with $\delta g_\parallel^{v_i}(F_z)$, see Eqs. (52), (54), and (72).

$$\varphi_{v_i} = \frac{1}{2}\arcsin\left(\frac{\alpha_{R;v_i}}{\beta_{D;v_i}}\right) \simeq \frac{\alpha_{R;v_i}}{2\beta_{D;v_i}} + k\frac{\pi}{2}, \quad k = 0, \pm1, \pm2, \ldots, \tag{53}$$

where the inequality $|\alpha_{R;v_i}| \ll |\beta_{D;v_i}|$ is assumed from tight-binding calculations [25,59]. The sweet spot angles are generally different for the two eigenvalley states v_i. At these angles the spin qubit is immune to the charge noise (via the electric field F_z, see Sec. IV E 3). However, at the same sweet spot angles, the qubit frequency cannot be manipulated as well. (From a qubit perspective, there should be a trade off, where one can keep the possibility to manipulate the qubit reasonably fast, and simultaneously minimize the noise.) There are weak second-order PT effects, to be considered in the next section. It is interesting to note that for a zero Dresselhaus contribution the g-factor variation $\delta g_\parallel^{v_i}$ becomes angle-independent.

For a linear z confinement, one can rewrite Eq. (51) as

$$\delta g_\parallel^{v_i}(\varphi,F_z) \equiv A_{v_i}(\varphi)F_z^{2/3}, \tag{54}$$

since the SOC constants $\alpha_{R;v_i}, \beta_{D;v_i} \propto F_z$, and the average of the z motion in the lowest subband is $\langle z\rangle \simeq 1.5587\,(\hbar^2/2m_l|e|F_z)^{1/3}$, see Eq. (12). In the experiment [13], where the magnetic field is parallel to the [110] direction (i.e., $\varphi = \pi/4$), one gets from Eq. (51):

$$\delta g_\parallel^{v_i}(\pi/4,F_z) = -\frac{(\alpha_{R;v_i} - \beta_{D;v_i})|e|}{\hbar\mu_{\rm B}}\langle z\rangle \tag{55}$$

(for a discussion of the gauge-invariance of this result, see Appendix C 2). The g-factor scales as $F_z^{2/3}$, which is close to a linear scaling over the range (∼6%) of the experimentally applied electric fields, see Fig. 3(b).

Since the in-plane g-factor correction, $\delta g_\parallel^{v_i}$, is proportional to $\alpha_{R;v_i}, \beta_{D;v_i}$, it is clear that for the two eigenvalley subspaces,

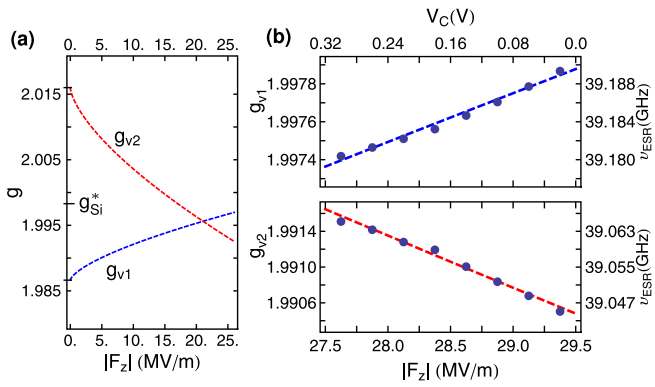

FIG. 3. In (a) the valley g-factors are plotted depending on the electric field F_z, based on the model, Eqs. (51), (55), and (71), for each eigenvalley state: $|v_1\rangle$, $|v_2\rangle$. The g-factor offsets at zero field and the intercept at $F_z^{\rm int} \simeq 2.1\times 10^7$ V/m are shown. In (b), the experimental electrical control over the valley g-factors is shown (dots, at a fixed magnetic field $B_0 = 1.4015$ T). The experimental points are fitted by the model, Eq. (71). Tuning both the confinement gate and the plunger gate at the QD [13] provides control of the electric field F_z, and with that we can vary the qubit resonance frequency over several MHz. The experimentally observed opposite dependence of the valley g-factors on the electric field is attributed to the mixing of the original bulk degenerate spin-valley wave functions at the Si/SiO_2 interface, via the dominance of the intervalley spin-flip contributions in the BC, Eqs. (6) and (9).

it may change sign along with the sign change of $\alpha_{R;v_i}$, $\beta_{D;v_i}$, Eq. (41). For example, for the intravalley spin-flip parameters being exactly zero, $s_R, s_D = 0$, the g-factor correction will be exactly opposite:

$$\delta g_\parallel^{v_1} = -\delta g_\parallel^{v_2}. \tag{56}$$

Relatively smaller corrections due to nonzero intravalley spin flipping, $s_R, s_D \neq 0$, will generally violate Eq. (56), leaving the g-factor corrections opposite in sign, but with different absolute value, $|\delta g_\parallel^{v_1}| \neq |\delta g_\parallel^{v_2}|$, which is observed in the current experiment [13], see Fig. 3. Tight-binding calculations [25] were performed for the case of a Si/SiGe interface, with the result that $|\chi_D| \gg |s_D|$, $|\chi_R| \gg |s_R|$, while $|\chi_R| \sim |s_D|$, supporting the case of Eqs. (41) and (56). For comparison of the results, Eqs. (51)–(55), with the experiment, see Sec. IV E.

2. $\delta g_\parallel$ to second-order PT

Since at certain angles of the in-plane magnetic field, Eq. (53), the g-factor first-order correction can be zeroed, one needs to calculate also higher order effects, which arise due to QD's energy level structure.

We consider a small quantum dot (QD) in MOS Si/SiO_2 heterostructure, Figs. 1(c) and 1(d). Thus the QD is designed such that the first excited orbital state for one-electron QD is at $\Delta_{\rm orb} \simeq 8$ meV above the ground state, and for the three-electron QD, $\Delta_{\rm orb} \simeq 2$ meV [7]. Since the valley splitting, $E_{\rm VS}$, between the lowest valley eigenstates $|v_1\rangle$ and $|v_2\rangle$ is of the order of few hundred μeV in such heterostructures, the structure of levels is that shown in Figs. 1(c) and 1(d), with the two closely spaced eigenvalley states separated by $\Delta_{\rm orb} \equiv \hbar\omega_0 \gg E_{\rm VS}$ from the first two orbital excited QD states (Appendix B). The shorthand notation $|\bar v_i\rangle \equiv |v_i\rangle \otimes |\phi_{v_i}(\boldsymbol{r})\rangle$, $i = 1, 2$, includes the eigenvalley state and the envelope wave function $|\phi_{v_i}(\boldsymbol{r})\rangle \equiv \phi_0^{v_i}(x, y)\varphi_0(z)$ of the electron confined in the QD. The envelope wave function may depend on the valley index for a nonideal interface (with roughness) [7,40]. Similarly, the states $|m_1\rangle \equiv |v_1\rangle \otimes |0_x, 1_y, 0_z\rangle$ and $|m_2\rangle \equiv |v_1\rangle \otimes |1_x, 0_y, 0_z\rangle$, and $|\tilde m_1\rangle \equiv |v_2\rangle \otimes |0_x, 1_y, 0_z\rangle$ and $|\tilde m_2\rangle \equiv |v_2\rangle \otimes |1_x, 0_y, 0_z\rangle$, include first orbitally excited states. The states $|m_1\rangle$, $|m_2\rangle$ as well as $|\tilde m_1\rangle$, $|\tilde m_2\rangle$ are degenerate for a circular QD [51], and split from each other by $E_{\rm VS}$. We will neglect higher orbital excitations, assuming parabolic lateral confinement [see Fig. 1(d)].

In a magnetic field, each of these levels are Zeeman split, with $E_Z = g^* \mu_B B$, and we enumerate them as $|1\rangle, |2\rangle \ldots, |12\rangle$ (e.g., $|1\rangle \equiv |\bar v_1, \downarrow\rangle$, $|2\rangle \equiv |\bar v_1, \uparrow\rangle$, $|3\rangle \equiv |\bar v_2, \downarrow\rangle$, $|4\rangle \equiv |\bar v_2, \uparrow\rangle$, $|5\rangle \equiv |m_1, \downarrow\rangle$, $|6\rangle \equiv |m_1, \uparrow\rangle$, etc.). In fact, $|2\rangle = |\bar v_1, \uparrow\rangle$ and $|3\rangle = |\bar v_2, \downarrow\rangle$ anticross at $E_Z = E_{\rm VS}$ (for notations see below and in Appendix B) with energy splitting [7,8] $2|V_{23}| \equiv \Delta_a \simeq \frac{\sqrt{2}m_t E_{\rm VS}|\beta_D^{12} - \alpha_R^{12}|}{\hbar}(x_{12} + y_{12})$ in the presence of interface roughness [7,8], and due to the effective Rashba and Dresselhaus SOC interaction Hamiltonians, $\mathcal{H}_{\rm s\text{-}v}^{ij}$ Eq. (34). Using this level structure, one is able to describe successfully the experimentally observed "relaxation hot spot" that occurs in the region of maximal spin-valley mixing [7], at $E_Z \approx E_{\rm VS}$ (where the phonon relaxation is strong). Moreover, the standard SOC corrections via the virtual excitation to the orbital levels $|m_{1,2}\rangle$ describe correctly the B^7 magnetic field dependence of the relaxation rate above the anticrossing [7], at $E_Z > E_{\rm VS}$. (For a three-electron QD, the structure of levels is essentially the same, Fig. 1(c): this explains essentially the experimentally identical "relaxation hot spot" measured in the 3e-system [7]).

For the second-order correction to the g-factor of the lower valley (v_1) electron, $\delta^{(2)} g_\parallel^{v_1} = [\delta E_2^{(2)} - \delta E_1^{(2)}]/(\mu_B B_\parallel)$, we use standard perturbation theory for the energy difference $[\delta E_2^{(2)} - \delta E_1^{(2)}]$ (Appendix B 1).

$$\begin{aligned}\delta E_2^{(2)} - \delta E_1^{(2)} &= \frac{2|V_{12}|^2}{E_Z} + |V_{14}|^2\left(\frac{1}{E_Z - E_{\rm VS}} + \frac{1}{E_Z + E_{\rm VS}}\right) \\ &+ 2|V_{16}|^2\left(\frac{1}{E_Z - \Delta_{\rm orb}} + \frac{1}{E_Z + \Delta_{\rm orb}}\right) + 2|V_{1,10}|^2 \\ &\times\left(\frac{1}{E_Z - \Delta_{\rm orb} - E_{\rm VS}} + \frac{1}{E_Z + \Delta_{\rm orb} + E_{\rm VS}}\right).\end{aligned} \tag{57}$$

The matrix elements V_{ab}, $a = 1, 2$, $b = 1, \ldots, 12$, are routinely calculated, using the relation between matrix elements of momentum and position via the equation of motion. In Eq. (57), we have used that $V_{23} = V_{14}$, $V_{25} = V_{16}$, $V_{27} = V_{18}$, etc., and also that $V_{16} = V_{18}$, $V_{1,10} = V_{1,12}$ for a circular dot (Appendix B 1). SOCs, Eq. (34), make the qubit states, $|1\rangle \equiv |\bar v_1, \downarrow\rangle$, $|2\rangle \equiv |\bar v_1, \uparrow\rangle$, to mix with the upper orbital states $|m_1\rangle$, $|m_2\rangle$, $|\tilde m_1\rangle$, $|\tilde m_2\rangle$, as well as with the $|\bar v_2\rangle$ states. The mixing to the $|\bar v_2\rangle$ states (which have a quasi s-like envelope) is via the transition dipole matrix elements $\boldsymbol{r}_{12} \equiv \langle \bar v_1|\boldsymbol{r}|\bar v_2\rangle$ (notice, $\boldsymbol{r}_{12} \neq 0$ only due to roughness effects [7,40]), and the mixing to the higher orbital states $|m_i\rangle$, $|\tilde m_i\rangle$ is via the standard orbital dipole matrix elements, i.e., $\boldsymbol{r}_{1,m_1} \equiv \langle v_1|\boldsymbol{r}|m_1\rangle$, etc.;

for a circular dot, $y_{1,m_1} = x_{1,m_2} = \sqrt{\frac{\hbar^2}{2m_t\Delta_{\rm orb}}}$ (also, we assume $y_{1,\bar{m}_1} = x_{1,\bar{m}_2} \simeq y_{1,m_1}$).

Here we present the approximate result (for exact expressions, see Appendix B 1), assuming $x_{12} = y_{12} \sim \langle z\rangle \simeq$ few nm, and SOC constant relations suggested by the tight-binding calculations: $\alpha_{R;v_1} \ll \beta_{D;v_1}$, and $|\alpha_{R;21}| \ll |\beta_{D;21}|$. For the relevant (to the experiment) case of $E_Z \ll E_{\rm VS}, \Delta$ one gets

$$\delta^{(2)}g_\parallel^{v_1} \simeq \frac{|e|^2}{\hbar^2\mu_B^2}\Big\{\beta_{D;v_1}^2\cos^2 2\varphi\,\langle z\rangle^2 - (m_t/m_0)^2 \times\Big[|\beta_{D;21}|^2(1+\sin 2\varphi)\,x_{12}^2 + \big(\beta_{D;v_1}^2 + |\beta_{D;21}|^2\big)\,y_{1m_1}^2\Big]\Big\}. \tag{58}$$

In Eq. (58), the first term ($\sim\langle z\rangle^2$) is exact and can be extracted from the second-order expansion of Eq. (50) for $v_i = v_1$ [it is zero in the [110] direction]. It can be seen that the whole second-order correction is of the order of $|\delta^{(2)}g_\parallel^{v_1}| \sim [\delta^{(1)}g_\parallel^{v_1}]^2 \sim 10^{-6}$. (We assume that similar relation holds for the v_2 electrons, without calculation.)

The smallness of the second order contribution can be also seen by noting that the second term ($\sim x_{12}^2$) and the third term ($\sim y_{1m_1}^2$) in Eq. (58) are proportional to the small ratios $|\Delta_a|^2/E_{\rm VS}^2$ and $|V_{16}|^2/\Delta_{\rm orb}^2 = m_t|\beta_{D;21} - \alpha_{R;21}|^2/(4\Delta_{\rm orb})$ that are of the order of 10^{-6}–10^{-8}, since the splitting at the spin-valley anticrossing is small [7,8], $\Delta_a \approx (10^{-3} - 10^{-4})E_{\rm VS}$.

At the spin-valley anticrossing, $E_Z \approx E_{\rm VS}$, the g-factor change is somewhat bigger, $|\delta g| \sim \Delta_a/E_{\rm VS}$, which is still at least one order of magnitude smaller than is experimentally observed. Moreover, the electric field dependence in F_z arising from this contribution is nonlinear, which is not observed experimentally [13] (Appendix B 3). This experimental fact restricts the size of the spin-valley splitting at the anticrossing point [7]. Also notice that due to quadratic dependence on the SOC constants this contribution would be insensitive to the change of their sign.

C. g-factor for perpendicular magnetic field $B_\perp$

1. $\delta g_\perp$ to first-order PT

For a perpendicular magnetic field one chooses the gauge $\boldsymbol{A}_\perp(\boldsymbol{r}) = \frac{B_z}{2}(-y, x, 0)$; In what follows, we again neglect small corrections originating from the bulk Hamiltonian $\mathcal{H}_0$, Eq. (12). The perturbation to Eq. (42), $\delta_B\mathcal{H}_{v_i}^{\rm 3D}$, due to perpendicular magnetic field $\boldsymbol{B}_\perp$, contributes to $\delta g_\perp$ to first order. Averaging it over the states $|\bar{v}_i\rangle$ as in Eq. (45) gives

$$\big\langle\bar{v}_i\big|\delta_B\mathcal{H}_{v_i}^{\rm 3D}\big|\bar{v}_i\big\rangle = \frac{|e|}{\hbar\mu_B}\,\mu_B\frac{B_z}{2}[\alpha_{R;v_i}(\sigma_x x_{11} + \sigma_y y_{11}) - \beta_{D;v_i}(\sigma_x y_{11} + \sigma_y x_{11})],\quad i = 1, 2. \tag{59}$$

Similar to Eq. (47) the total Zeeman energy can be written via the g-factor tensor:

$$\mathcal{H}_{{\rm Z},v_i}^{\rm tot} = \mu_B\frac{B_z}{2}\big(g_0\sigma_z + \delta g_{xz}^{v_i}\sigma_x + \delta g_{yz}^{v_i}\sigma_y\big), \tag{60}$$

where

$$\delta g_{xz}^{v_i} = \frac{|e|}{\hbar\mu_B}(\alpha_{R;v_i}x_{11} - \beta_{D;v_i}y_{11}), \tag{61}$$

$$\delta g_{yz}^{v_i} = \frac{|e|}{\hbar\mu_B}(\alpha_{R;v_i}y_{11} - \beta_{D;v_i}x_{11}), \tag{62}$$

and $\boldsymbol{r}_{11} \equiv \langle\bar{v}_1|\boldsymbol{r}|\bar{v}_1\rangle$. These contributions would be zero for an ideal interface, while they may be nonzero for an interface with roughness, e.g., due to atomic steps [7,40]. In fact, just these matrix elements are needed in order to explain the "relaxation cold spot" for a QD with two electrons [7]. The first-order correction, however, is zeroed as the perturbation is off-diagonal in spin.

2. $\delta g_\perp$ to second-order PT

Exact diagonalization of (60) allows to extract a partial second-order contribution, similar to Eqs. (50) and (58):

$$\delta g_\perp^{v_i} = \frac{|e|^2}{\hbar^2\mu_B^2}\frac{1}{2g^*}\big\{\big(x_{11}^2 + y_{11}^2\big)\big(\alpha_{R;v_i}^2 + \beta_{D;v_i}^2\big) - 4x_{11}y_{11}\alpha_{R;v_i}\beta_{D;v_i}\big\}. \tag{63}$$

Adding the contributions of the higher levels and using the same approximations as in subsection IV B 2, just before Eq. (58), we obtain (Appendix B 2):

$$\delta^{(2)}g_\perp^{v_1} \simeq \frac{|e|^2}{\hbar^2\mu_B^2}\Big\{\beta_{D;v_1}^2\frac{x_{11}^2}{2} - 2(m_t/m_0)^2(m_0/m_t - 1) \times\big[\beta_{D;v_1}^2\big(x_{12}^2 + y_{1m_1}^2\big) + |\beta_{D;21}|^2\,y_{1m_1}^2\big]\Big\}. \tag{64}$$

In Eq. (64), the first term ($\sim x_{11}^2$) is exact and is taken from Eq. (63). It can be seen again that the whole expression is of the order of $|\delta^{(2)}g_\perp| \sim [\delta^{(1)}g_\parallel]^2 \sim 10^{-6}$.

D. g-factor total angular dependence

To leading order in $a[U_z]$, and neglecting the contributions, Eqs. (61) and (62), the effective g-factor correction is obtained from Eqs. (45) and (60) and reads

$$\delta g^{v_i}(\varphi,\theta) \simeq -\frac{|e|}{\hbar\mu_B}\frac{\langle z\partial_z U_z\rangle}{\langle\partial_z U_z\rangle}\,(\alpha_{R;v_i} - \beta_{D;v_i}\sin 2\varphi)\sin^2\theta, \tag{65}$$

where the magnetic field components are chosen as: $\boldsymbol{B} = B(\sin\theta\cos\varphi, \sin\theta\sin\varphi, \cos\theta)$. Corrections from the matrix elements, Eqs. (61) and (62), give an additional contribution with a different angular dependence:

$$\delta g_\perp^{v_i}(\varphi,\theta) \simeq -\tfrac{1}{2}\sin 2\theta\big(\cos\varphi\ \delta g_{xz}^{v_i} + \sin\varphi\ \delta g_{yz}^{v_i}\big). \tag{66}$$

However, the preservation of the C_{2v} symmetry would exclude roughness/steps within the dot, thus eliminating the latter contribution.

E. Discussion of the results and comparison to experiment

1. Angular dependence

Our predicted g-factor angular dependence (see Fig. 2) of the leading contributions for an applied magnetic field,

both in-plane, Eq. (51), and perpendicular to the interface, Eq. (65), was recently confirmed in an experiment using a Si-MOS DQD structure [16]. In the DQD experiment [16], the singlet-triplet qubit is manipulated via the energy detuning between the dots which translates in different perpendicularly applied electric fields at each dot, and therefore to a different g-factor, Eq. (51). The measured angular dependence, both in-plane and out-of-plane, is compatible with the predicted $\sim \sin 2\varphi \sin^2\theta$ angular dependence of Eq. (65) [see also Eq. (51)]. The angle φ_{v_1}, Eq. (53), at which the g-factor correction is zero, allows essentially to extract the ratio of the Dresselhaus versus Rashba constants for the lowest eigenvalley band v_1: $\beta_{D;v_1}/\alpha_{R;v_1} \approx 8.3$, at the conditions of the experiment [16]. The smallness of the calculated by us second-order corrections to the g-factor, Eqs. (58) and (64), including that coming from the QD level structure, is consistent both with the single QD experiment [13] and with the recent DQD experiment [16,18].

2. Valley dependence

While the single QD experiment [13] was performed for a fixed in-plane magnetic field along the crystallographic [110] direction, it has revealed important information about the valley dependence of the g-factor, predicted in Eqs. (51) and (55). Indeed, because of the strong lateral confinement, the orbital splitting is much larger than the valley splitting, $\Delta_{\rm orb} \gg E_{\rm VS}$, and it is now clear that if the Si QD is occupied by a single electron, then one is measuring the $g_{\rm v_1}$-factor of the lower valley state, $|v_1\rangle$, Fig. 1(c), left. For a QD occupied by three electrons, Fig. 1(c), right, the "valence" electron is at the upper valley eigenstate $|v_2\rangle$, and thus $g_{\rm v_2}$ is effectively measured. Despite the smallness of the g-factor change as a function of the applied electric field, the corresponding energy change can be resolved since it happens to be ~3000 times larger than the corresponding ESR linewidth of 2.4 kHz. The electric field dependence allows the spin qubit evolution to be switched on/off by tunning it in/out of resonance with an external microwave drive [11,13].

Let us perform a rough estimation of the 2D spin-orbit parameters, $\alpha_{R;v_i}$, $\beta_{D;v_i}$, based on the measured g-factor dependencies, Fig. 3(b), and using the predicted electric field dependence in the range of high electric fields, $\delta g^{\rm th}_{\rm v_i} = A_{v_i} F_z^{2/3}$, Eqs. (54) and (55). The measured change of the $g(F_z)$-factors is approximately a linear function of the electric field F_z for the experimental electric field range, $F_z \approx (2.75\text{–}2.95) \times 10^7$ V/m, and $g_{\rm v_1}(F_z)$ grows with increasing F_z [Fig. 3(b), upper panel], while $g_{\rm v_2}(F_z)$ decreases [Fig. 3(b), lower panel]. The experimental energy change of 10–20 MHz corresponds to g-factor changes, $\Delta[\delta g_{\rm v_1}]$, $\Delta[\delta g_{\rm v_2}] \approx 10^{-3}$. Moreover, the measured g-factor changes *are opposite in sign*, and fulfill the approximate relation

$$\Delta\big[\delta g^{\rm exp}_{\rm v_2}(F_z)\big] \simeq -2.24\ \Delta\big[\delta g^{\rm exp}_{\rm v_1}(F_z)\big], \tag{67}$$

which was qualitatively explained in Sec. IV B 1 via the *dominance of the intervalley spin-flip scattering amplitudes* over the intravalley spin-flip amplitudes in the BC, Eq. (6). Since $\Delta[\delta g^{\rm exp}_{\rm v_2}(F_z)]/\Delta[\delta g^{\rm exp}_{\rm v_1}(F_z)] = A_{v_2}/A_{v_1}$ (for high fields), one can extract the ratio

$$\frac{A_{v_2}}{A_{v_1}} = \frac{\alpha_{R;v_2} - \beta_{D;v_2}}{\alpha_{R;v_1} - \beta_{D;v_1}}\bigg|_{\rm high-field,\varphi=\frac{\pi}{4}} \simeq -2.24. \tag{68}$$

Moreover, expanding $\delta g_{\rm v_i}$ to second order: $\Delta[\delta g_{\rm v_i}] \simeq A_{v_i} F_z^{2/3} \frac{2}{3}(\frac{\Delta F_z}{F_z} - \frac{1}{3}\frac{\Delta F_z^2}{F_z^2})$, with $\Delta F_z = 0.175 \times 10^7$ V/m [Fig. 3(b)] and, using Eqs. (51) and (55), one obtains

$$\alpha_{R;v_1} - \beta_{D;v_1} \simeq -361 \times 10^{-13}\ {\rm eV\,cm}, \tag{69}$$

$$\alpha_{R;v_2} - \beta_{D;v_2} \simeq 810 \times 10^{-13}\ {\rm eV\,cm} \tag{70}$$

(with a relative error of 5×10^{-4}; however, a systematic error due to deviation from the high-field behavior, $\sim F_z^{2/3}$, is not accounted). These values are compatible with qualitative estimations for GaAs heterojunctions [1], and also with tight-binding calculations of Nestoklon *et al.* [25] for a Si/Ge interface. They are larger than the latter by a factor of 10, which is expected since here the electric field is ~3 times higher than in that calculations, and the Si/SiO_2 interface is more abrupt.

Finally, we would like to stress that the g-factor dependence of $F_z^{2/3}$ is for a high electric field (see Sec. III B). Thus, we will model the low-field dependence in a simplistic way, by adding a (valley-dependent) g-factor offset δx_{v_i} [Fig. 3(a)]:

$$g_{\rm v_i} = g^*_{\rm Si} + \delta x_{v_i} + A_{v_i} F_z^{2/3}, \tag{71}$$

where $g^*_{\rm Si} \simeq 1.9983$ is the bulk value in Si for in-plane magnetic field [20,21,56]. By fitting Eq. (71) to the experimental data, Fig. 3(b), one obtains the g-factor offsets $\delta x_{v_1} \simeq -0.012$, and $\delta x_{v_2} \simeq 0.018$ (with an error of 5×10^{-4}), for this particular angle $\varphi = \pi/4$, when $B_\parallel$ is along the [110] direction. We note that the assumed C_{2v}-symmetry of the interface (quantum well) implies that the low-electric field Hamiltonian will be described by the same invariant Rashba and Dresselhaus structures, see Eq. (34). This would imply some $\sim \sin 2\varphi$ dependence of the offset values, reflecting the symmetry. A theory of the low-electric field effects in the g-factors, including offsets will be considered elsewhere.

While an interface with roughness (which is a realistic interface) will generally violate the "global" C_{2v} symmetry, one might expect, for relatively small dots, a situation when the C_{2v} symmetry is not violated within the quantum dot. This symmetry will dictate the form of the interface Hamiltonian, e.g., in Eq. (34), and the g-factor angular dependence, derived in Eqs. (51) and (65). This physical intuition was recently confirmed experimentally, by observing the angular dependence in a Si-MOS DQD experiment [16,18]. Similar angular dependence was also revealed in a single QD with micromagnet, manipulated at a Si/Ge interface [14]. We stress that any explicit violation of the C_{2v} symmetry (e.g., via explicit atomic step in the QD [15]) will not result in the angular dependence predicted here for the g-factor, Eq. (51); moreover, one would not be allowed to speak about Rashba and Dresselhaus contributions in the Hamiltonian. More experimental and theoretical work is needed to understand the role of atomic steps/roughness on the g-factor and other parameters.

3. Spin-orbit coupled electric field noise

The F_z dependence of the g-factor implies that a new dephasing mechanism is introduced via the fluctuations of the (gate) electric field, which was discussed in the context of 1e- and 3e-qubit using randomized benchmarking sequences to reveal it [13,60,61]. For the single QD qubit of Ref. [13], this is the detuning noise $\delta\epsilon(t)$ of the Hamiltonian $\mathcal{H}_{Qb} = \frac{\epsilon}{2}\sigma_z + \frac{B_1^{\rm ac}}{2}\sigma_x$, where $\epsilon \propto \nu_{\rm ESR} - \nu_{v_i}$ is the detuning, and $B_1^{\rm ac}$ is the ac driving amplitude. Assuming a white noise, $\delta\epsilon(t) = \xi_\epsilon(t)$ with a (single-sided) noise spectral density S_ϵ, (see, e.g., Ref. [62]), the dephasing rate γ_{v_i} is derived at a chosen field F_{z0}^* as

$$\gamma_{v_i} = \frac{S_\epsilon}{4\hbar^2} = \frac{(\mu_B B_\parallel)^2}{4\hbar^2}\left|\frac{\partial[\delta g_\parallel^{v_i}(\varphi, F_{z0}^*)]}{\partial F_z}\right|^2 a^2 S_V, \qquad (72)$$

where S_ϵ is linearly related to the gate voltage spectral density S_V, assuming linear dependence of field versus voltage, $F_z \equiv a\,V$ (see, Fig. 3(b) and Ref. [7]). From Eq. (52), one obtains suppression for high fields, e.g., for a linear confinement: $\frac{\partial[\delta g_\parallel^{v_i}(\varphi,F_z)]}{\partial F_z} = \frac{1}{F_z}\delta g_\parallel^{v_i}(\varphi, F_z)$. Using Eq. (67), the dephasing rates for the 3e and 1e qubits (for $\varphi = \pi/4$) should be related as $\gamma_{v_2} \simeq (2.24)^2\,\gamma_{v_1}$. On the other hand, using Hahn echo measurements one can cancel out the $1/f$ (drift) noise, and the measured T_2 reveals $T_2^{3e} \approx 400\mu s$ and $T_2^{1e} \approx 1200\mu s$, i.e., a dephasing rate ratio of 3 instead of $(2.24)^2$. This can be explained assuming another (valley-independent) dephasing γ_0 (it can be associated with some charge fluctuators or noise on the ac amplitude $B_1^{\rm ac}$). Thus $\gamma_{3e} = \gamma_{v_2} + \gamma_0$, $\gamma_{1e} = \gamma_{v_1} + \gamma_0$, with $\gamma_0 \simeq \gamma_{v_1}$, i.e., γ_0 is comparable to γ_{v_1} in this experiment.

The quadratic dependence of the noise on the g-factor change: $S_\epsilon \propto [\delta g_\parallel^{v_i}(\varphi, F_z)]^2$, Eqs. (52) and (72), implies that it can be zeroed at the "sweet spot angles" φ_{v_i}, defined in Eq. (53). At these angles (which may be different for the two eigenvalley subspaces, v_1, v_2), either γ_{1e} or γ_{3e} will take the minimal value γ_0. Similar decrease of the noise can be achieved by rotating the field perpendicular to the interface since the g-factor corrections are strongly suppressed, see Eqs. (63) and (64).

V. SUMMARY AND DISCUSSION

This paper presents a detailed theory to explain measurements of unexpected g-factor shifts in silicon quantum dots and to predict future experiments and impact to silicon-based quantum computing. We derived the effective spin-orbit interaction from appropriately formulated boundary conditions that take into account the symmetry of the silicon heterostructure interface and the hermiticity of the problem at hand. These effective spin-orbit interactions are used to derive the valley splitting at the interface, both its scaling with the applied electric field (perpendicular to the interface) and with the interface z confinement for the conduction electrons. Then the 3D (and 2D) effective Rashba and Dresselhaus spin-orbit interactions are calculated, assuming a C_{2v} interface symmetry. We argue that these new interface SOC contributions are much stronger than possible bulk contributions. Compared to previous phenomenological approaches [7,8,10,24,26,50,51,63–67], the approach taken in this paper provides more rigorous ground for analyzing current and future experiments.

The effective spin-orbit interactions contain both diagonal (in the eigenvalley number) and off-diagonal contributions, which are to be used in the analysis of experiments that involve both eigenvalley states (e.g., in the so-called valley qubits [68,69]). Based on the above, we derived the electron g-factors for conduction 2DEG electrons (at a relatively weak lateral confinement) for an applied in-plane or perpendicular to the interface magnetic field. To leading order, we predicted the angular dependence of the g-factor with the in-plane angle, as well as with the azimuthal angle (for a magnetic field having a perpendicular component). For appropriate experiments with a single QD, these predictions would allow us to extract the ratio of Rashba and Dresselhaus effective constants, from a measured g-factor angular dependence. In fact, any significant angular dependence will show that the Dresselhaus contribution dominates the Rashba one, thus supporting our statement that interface contributions are much stronger than that originating from the bulk.

The physical mechanism that causes shifts in the SOC parameters (and thus g-factor) as a function of electric field allows a new path for charge noise to affect the qubit. The predictions in this paper on the g-factor angular dependence are made for both lower and upper eigenvalley subspaces, which in general may have different spin-orbit (Rashba and Dresselhaus) contributions. We predict, based on the in-plane angular dependence, the so-called *sweet spots in the direction of the magnetic field, when the g-factor correction, δg is zero*, and therefore there is no electric field scaling; consequently, the corresponding spin qubit would be insensitive (to first order) to the gate voltage (charge noise) of the applied electric field mediated by these new SOC contributions. As a trivial consequence, a QD *qubit will be also insensitive to gate (charge) noise when the magnetic field is perpendicular to the interface*, as in this case the g-factor variation is equally suppressed. To estimate this suppression, we have also calculated the second-order corrections (in the perturbation theory) to the g-factor at any magnetic field direction, which also include the effects of the internal QD level structure, assuming strong confinement typical for the current experiments [8,11,13,16,18]. We have shown that these corrections are typically small $\sim 10^{-6}$ which supports the first order results discussed above. Eventually, an enhancement of these effects is possible near the so-called "relaxation hot spot" [7], where the g-factor corrections may reach $\sim 10^{-4}$–10^{-3}, however, such enhancement was not observed experimentally [11,13]. The absence of such enhancement may be explained (is consistent) with our theory, giving further constraints on the interface BC matrix parameters (both of their amplitudes and phases).

The ability to appreciably change the g-factor of an electron via applied voltages on top-gates offers a new and unplanned-for opportunity for control of silicon quantum dot qubits. For example, implementing a two-qubit encoding [70] would allow for all-electrical control without the need for three-quantum dots, magnetic field, or nuclear gradients; this may be relevant for quantum computing not only in reducing the overhead in qubits but also in gate pulses as, for example, it has been recently showed that two-qubit encoded gates can

be accomplished in far fewer gates than 2-DFS encodings [71]. Further, the fact that one electron and three electron dots exhibit different behavior (while both still being good qubits) provides another opportunity for creative quantum dot gate protocols. On the other hand, g-factor tunability can create new mechanisms for decoherence, especially an increased sensitivity to charge noise. Our theory predicts a means to remove this channel by magic magnetic field angles (perpendicular, for example). Finally, we note that the above theory should also apply to Si/Ge heterostructure quantum dots, with the caveat that the shift in g-factor will likely be smaller relative to the MOS-interface dots.

Note added. While we were preparing our manuscript [57,58], we became aware of a relevant experiment on a MOS double quantum dot system [16] (and most recently see the experiment [18]) at the similar conditions discussed in our paper, dealing with the lowest eigenvalley states in the DQD. Namely, their conditions are at an applied perpendicular to the interface electric field and at a magnetic field applied at various angles (both in-plane and perpendicular). The new experimental results of Ref. [16] confirm to a large extent our predictions.

Particularly, (i) the very possibility to manipulate the singlet-triplet DQD qubit is via the difference in the electron g-factor in the two dots, which arises in the deep (1, 1) regime, where the electric field applied to each of the dots becomes essentially different (i.e., far from the symmetric/degeneracy point); (ii) their observed angular dependence, $\sim \sin 2\varphi$ is compatible with our predictions for the lower eigenvalley subspace, see Eq. (51). (iii) Since the difference of the Dresselhaus and Rashba effective spin-orbit couplings, for the two dots, is linear with the dots' electric field difference, the ratio of $\Delta\beta/\Delta\alpha \approx 8.3$ extracted in the DQD experiment [16] is exactly the ratio of these couplings (that is independent of the electric field strength) $\beta_{D;v_1}/\alpha_{R;v_1}$, for the lower eigenvalley subspace, see Eqs. (35) and (36). (iv) Finally, we mention that the predicted in our paper angular dependence of the dephasing, having a minimum dephasing rate at the "sweet spot angles," Eq. (53), is yet to be measured in an experiment.

ACKNOWLEDGMENTS

A.S.D. acknowledges support from the Australian Research Council (CE11E0001017 and CE170100039) and the US Army Research Office (W911NF-13-1-0024 and W911NF-17-1-0198). The views and conclusions contained in this document are those of the authors and should not be interpreted as representing the official policies, either expressed or implied, of the Army Research Office or the US Government. The US Government is authorized to reproduce and distribute reprints for Government purposes notwithstanding any copyright notation herein.

APPENDIX A: DERIVATION OF THE EFFECTIVE SURFACE HAMILTONIAN FROM BOUNDARY CONDITIONS

In this appendix, we derive Eq. (18). Starting with the boundary condition (6), one denotes it as $\mathcal{B}\Phi\,|_{z=z_0^+}=0$ with $\mathcal{B}\equiv\mathcal{B}_1+\mathcal{B}_2$, and $\mathcal{B}_1\equiv 1+i\,R\,k_z$, $\mathcal{B}_2\equiv -R\frac{2m_l}{\hbar^2}V_{\rm if}(\boldsymbol{k})$; $V_{\rm if}(\boldsymbol{k})$ being the interface spin-valley mixing matrix. Since $\langle k_{x,y}^2\rangle \ll \langle k_z^2\rangle$ (for a strong z confinement), we will consider $\mathcal{B}_2$ as a perturbation. In what follows, we will approximately replace the boundary operator $\mathcal{B}$ by a unitary one up to higher order corrections:

$$\mathcal{B}\simeq\Gamma_{\rm BC}, \tag{A1}$$

with $\Gamma_{\rm BC}\,\Gamma_{\rm BC}^{\dagger}\simeq 1$.

Indeed, to zeroth order, we have the BC $\mathcal{B}_1\Phi^{(0)}\,|_{z=z_0^+}=0$, see Eq. (26). Then it follows that

$$\mathcal{B}_2\,\mathcal{B}_1\Phi^{(0)}\,|_{z=z_0^+}=0 \tag{A2}$$

or

$$\mathcal{B}_2\Phi^{(0)}\,|_{z=0^+}=\mathcal{B}_2\,(1-\mathcal{B}_1)\Phi^{(0)}\,|_{z=z_0^+}\,. \tag{A3}$$

Now, to first order, one has

$$\mathcal{B}\Phi\,|_{z=z_0^+}=[\mathcal{B}_1\,(\Phi^{(0)}+\Phi^{(1)})+\mathcal{B}_2\,\Phi^{(0)}]\,|_{z=z_0^+}=0 \tag{A4}$$

or

$$[\mathcal{B}_1\,\Phi(z)+\mathcal{B}_2\,(1-\mathcal{B}_1)\Phi(z)]\,|_{z=z_0^+}=0, \tag{A5}$$

where we have replaced $\Phi^{(0)}$ by Φ in the second term of Eq. (A4) up to higher-order corrections. The last BC, Eq. (A5), can be rewritten in the form $\Gamma_{\rm BC}\Phi(z)\,|_{z=z_0^+}=0$, where

$$\Gamma_{\rm BC}=\mathcal{B}_1+\mathcal{B}_2\,(1-\mathcal{B}_1)=1+i\,\gamma_{\rm BC}, \tag{A6}$$

$$\gamma_{\rm BC}\equiv R\,k_z+R^2\frac{2m_l}{\hbar^2}V_{\rm if}(\boldsymbol{k})\,k_z, \tag{A7}$$

and $\Gamma_{\rm BC}$ is an (approximate) unitary operator, $\Gamma_{\rm BC}\,\Gamma_{\rm BC}^{\dagger}=1+\mathcal{O}(\gamma_{\rm BC}^2)$, up to higher orders.

Performing now the unitary transformation with $\Gamma_{\rm BC}$ as in Eq. (17), the transformed BC is $\tilde{\Phi}\,|_{z=z_0^+}\equiv\Gamma_{\rm BC}\Phi\,|_{z=z_0^+}=0$ and the transformed Hamiltonian reads

$$\begin{aligned}\tilde{\mathcal{H}}&=\Gamma_{\rm BC}\mathcal{H}_0\Gamma_{\rm BC}^{\dagger}\simeq\mathcal{H}_0+\delta\mathcal{H}+\mathcal{O}\big(\gamma_{\rm BC}^2\big),\\ \delta\mathcal{H}&=i[\gamma_{\rm BC},\mathcal{H}_0]_-=R\partial_z U_z+R^2\frac{2m_l}{\hbar^2}V_{\rm if}(\boldsymbol{k})\partial_z U_z.\end{aligned} \tag{A8}$$

APPENDIX B: QD LEVEL STRUCTURE AND ITS CONTRIBUTION TO THE g-FACTOR

In order to emphasize the tunneling Hamiltonian representation implied by Eq. (5), we rewrite the expressions for the lowest eigenvalley states, Eq. (22), to the form

$$|\bar{v}_{i;\sigma}\rangle=\frac{1}{\sqrt{2}}\begin{bmatrix}C_\sigma\\0\end{bmatrix}\phi_{v_i}^{+z}(\boldsymbol{r})+\left(\frac{\mp e^{-i\phi_V}}{\sqrt{2}}\right)\begin{bmatrix}0\\C_\sigma\end{bmatrix}\phi_{v_i}^{-z}(\boldsymbol{r}),\qquad i=1,2\,;\ \ \sigma=\uparrow,\downarrow, \tag{B1}$$

where the corresponding valley populations are $\alpha_{+z}^{v_1}=\frac{1}{\sqrt{2}}$, $\alpha_{-z}^{v_1}=-e^{-i\phi_V}\frac{1}{\sqrt{2}}$, $\alpha_{+z}^{v_2}=\frac{1}{\sqrt{2}}$, $\alpha_{-z}^{v_2}=+e^{-i\phi_V}\frac{1}{\sqrt{2}}$. Time reversal maintains the relations: $|\alpha_{+z}^{v_j}|=|\alpha_{-z}^{v_j}|$ and $\phi_{v_j}^{+z}(\boldsymbol{r})=\phi_{v_j}^{-z}(\boldsymbol{r})$. For the lowest energy envelopes, $\phi_{v_i}^{+z}(\boldsymbol{r})=\phi_0^{v_i}(x,y)\,\varphi_0(z)$, the dependence on the eigenvalley index v_i is due to interface roughness (atomic steps within the dot), and makes $\phi_0^{v_i}(x,y)$ to acquire a p-like contribution [7,40]. The corresponding four lowest states $|v_i\rangle\otimes|0_x,0_y,0_z\rangle\otimes$

$|\sigma\rangle \equiv |\bar{v}_i, \sigma\rangle$, are enumerated as $|1\rangle \equiv |\bar{v}_1, \downarrow\rangle$, $|2\rangle \equiv |\bar{v}_1, \uparrow\rangle$, $|3\rangle \equiv |\bar{v}_2, \downarrow\rangle$, $|4\rangle \equiv |\bar{v}_2, \uparrow\rangle$, see Sec. IV B 2. The higher orbital states, Fig. 1(d), $|v_i\rangle \otimes |1_x, 0_y, 0_z\rangle \otimes |\sigma\rangle$, $|v_i\rangle \otimes |0_x, 1_y, 0_z\rangle \otimes |\sigma\rangle$, are enumerated using the notations $|m_1\rangle \equiv |v_1\rangle \otimes |1_x, 0_y, 0_z\rangle$, $|m_2\rangle \equiv |v_1\rangle \otimes |0_x, 1_y, 0_z\rangle$, and $|\tilde{m}_1\rangle, |\tilde{m}_2\rangle$ for $v_1 \to v_2$, namely, $|5\rangle \equiv |m_1, \downarrow\rangle$, $|6\rangle \equiv |m_1, \uparrow\rangle$, $|7\rangle \equiv |m_2, \downarrow\rangle$, $|8\rangle \equiv |m_2, \uparrow\rangle$, $|9\rangle \equiv |\tilde{m}_1, \downarrow\rangle$, $|10\rangle \equiv |\tilde{m}_1, \uparrow\rangle$, $|11\rangle \equiv |\tilde{m}_2, \downarrow\rangle$, and $|12\rangle \equiv |\tilde{m}_2, \uparrow\rangle$, see Sec. IV B 2. The roughness effects for these states are neglected. Also, higher orbital states are not considered assuming a close-to-parabolic lateral confinement.

We consider the valley diagonal SOC Hamiltonian (42) in a 3D form (since the 2D SOC Hamiltonians are generally inconsistent with the extension of derivatives). By suitably rotating the axes for an in-plane magnetic field, $\boldsymbol{B}_\parallel = (B_x, B_y, 0)$, one obtains

$$\mathcal{H}_{v_i} = [\alpha_{R;v_i}\{(s\tilde{\sigma}_x + c\tilde{\sigma}_z)P_y + (c\tilde{\sigma}_x - s\tilde{\sigma}_z)P_x\} + \beta_{D;v_i}\{(s\tilde{\sigma}_x + c\tilde{\sigma}_z)P_y + (c\tilde{\sigma}_x - s\tilde{\sigma}_z)P_x\}]\frac{\partial_z U_z}{\hbar\langle\partial_z U_z\rangle}, \tag{B2}$$

where $s \equiv \sin\varphi$, $c \equiv \cos\varphi$, $\boldsymbol{P} = \hbar\boldsymbol{k} + |e|\boldsymbol{A}$ are the extended derivatives, $B_x = B\cos\varphi$, $B_y = B\sin\varphi$, and the Pauli matrices along the new axes are

$$\tilde{\sigma}_z = \frac{\sigma_x B_x + \sigma_y B_y}{B}, \quad \tilde{\sigma}_x = \frac{\sigma_x B_y - \sigma_y B_x}{B} \tag{B3}$$

with $\tilde{\sigma}_z|\uparrow,\downarrow\rangle = \pm|\uparrow,\downarrow\rangle$ and $\tilde{\sigma}_x|\uparrow,\downarrow\rangle = |\downarrow,\uparrow\rangle$.

Taking the matrix elements $V_{kk} = \langle k|\mathcal{H}_{v_1}|k\rangle$, $k = 1, 2$, one obtains for the first-order correction to the g-factor ($U_z = |e|F_z z$ for simplicity):

$$\delta^{(1)}g_\parallel^{v_1} = \frac{V_{22} - V_{11}}{\mu_B B} = -\frac{|e|}{\hbar\mu_B}\langle z\rangle(\alpha_{R;v_1} - \beta_{D;v_1}\sin 2\varphi). \tag{B4}$$

It is straightforward to see that for a three-electron QD, one can write the wave function as a Slater determinant (mean field approximation is implicit [50,72]), where two of the electrons are occupying the lowest orbital $|\bar{v}_1\rangle$, and the "valence" electron occupies the upper (split by $E_{\rm VS}$) orbital, $|\bar{v}_2\rangle$, Fig. 1(c). Then, the matrix element over the 3e wave function is reduced to a single-particle matrix element of the form $V_{kk} = \langle k|\mathcal{H}_{v_2}|k\rangle$, $k = 3, 4$, which leads to an expression for $\delta^{(1)}g_\parallel^{v_2}$ analogous to Eq. (B4), with the replacement $v_1 \to v_2$.

1. Second-order corrections: case of $\boldsymbol{B}_\parallel$

For the second-order corrections, it is convenient to introduce compact notations for the SOC constants, Eqs. (35)–(38): $a_{ii} \equiv \alpha_{R;v_i}$, $b_{ii} \equiv \beta_{D;v_i}$, $i = 1, 2$, and $a_{21} \equiv \alpha_{R;21}$, $b_{21} \equiv \beta_{D;21}$. The second-order corrections include transitions to higher states with different valley content; so, both diagonal and nondiagonal in valley SOC Hamiltonians, Eq. (34), contribute:

$$\mathcal{H}_{\text{s-v}}^{ij} = \frac{a_{ij}}{\hbar}(\sigma_x P_y - \sigma_y P_x) + \frac{b_{ij}}{\hbar}(\sigma_x P_x - \sigma_y P_y). \tag{B5}$$

Rotating the axes as above, one obtains for the first few matrix elements,

$$V_{12} = \langle\bar{v}_1,\downarrow|\mathcal{H}_{\text{s-v}}|\bar{v}_1,\uparrow\rangle = \hbar^{-1}\langle\phi^{v_1}(\boldsymbol{x})|a_{11}(cP_x + sP_y) + b_{11}(sP_x + cP_y)|\phi^{v_1}(\boldsymbol{x})\rangle, \tag{B6}$$

$$V_{13} = \langle\bar{v}_1,\downarrow|\mathcal{H}_{\text{s-v}}|\bar{v}_2,\downarrow\rangle = \hbar^{-1}\langle\phi^{v_1}(\boldsymbol{x})|a_{12}(sP_x - cP_y) - b_{12}(cP_x - sP_y)|\phi^{v_2}(\boldsymbol{x})\rangle, \tag{B7}$$

$$V_{14} = \langle\bar{v}_1,\downarrow|\mathcal{H}_{\text{s-v}}|\bar{v}_2,\uparrow\rangle = \hbar^{-1}\langle\phi^{v_1}(\boldsymbol{x})|a_{12}(cP_x + sP_y) + b_{12}(sP_x + cP_y)|\phi^{v_2}(\boldsymbol{x})\rangle, \tag{B8}$$

$$V_{15} = \langle\bar{v}_1,\downarrow|\mathcal{H}_{\text{s-v}}|m_1,\downarrow\rangle = \hbar^{-1}\langle\phi^{v_1}(\boldsymbol{x})|a_{11}(sP_x - cP_y) - b_{11}(cP_x - sP_y)|\phi^{m_1}(\boldsymbol{x})\rangle, \tag{B9}$$

$$V_{16} = \langle\bar{v}_1,\downarrow|\mathcal{H}_{\text{s-v}}|m_1,\uparrow\rangle = \hbar^{-1}\langle\phi^{v_1}(\boldsymbol{x})|a_{11}(cP_x + sP_y) + b_{11}(sP_x + cP_y)|\phi^{m_1}(\boldsymbol{x})\rangle, \tag{B10}$$

etc. The matrix elements V_{ab}, $a = 1, 2$, $b = 1, \ldots, 12$, are routinely calculated, using the relation between momentum and position matrix elements via the equation of motion. For example,

$$\langle\phi^{v_1}(\boldsymbol{x})|p_x|\phi^m(\boldsymbol{x})\rangle = \frac{im_t}{\hbar}\langle\phi^{v_1}(\boldsymbol{x})|[\mathcal{H}_{\text{tot}}, x]_-|\phi^m(\boldsymbol{x})\rangle = \frac{im_t}{\hbar}(E_1 - E_m)\langle\phi^{v_1}(\boldsymbol{x})|\,x\,|\phi^m(\boldsymbol{x})\rangle, \tag{B11}$$

and similarly for $\langle p_y\rangle$.

Using these relations and the gauge $\boldsymbol{A}_\parallel(\boldsymbol{r}) = (B_y z, -B_x z, 0)$, we calculate the matrix elements

$$V_{12} = -\frac{|e|}{\hbar}\beta_{D;v_1}\cos 2\varphi\,\langle z\rangle, \tag{B12}$$

$$V_{13} = \left\{\frac{a_{12}}{\hbar}\left[\frac{im_t}{\hbar}E_{\rm VS}(cy_{12} - sx_{12}) - B\langle z\rangle\right] + \frac{b_{12}}{\hbar}\left[\frac{im_t}{\hbar}E_{\rm VS}(cx_{12} - sy_{12}) - B\sin 2\varphi\,\langle z\rangle\right]\right\}, \tag{B13}$$

$$V_{14} = \left\{ -\frac{a_{12}}{\hbar}\left[\frac{im_t}{\hbar}E_{\rm VS}(cx_{12}+sy_{12})\right] - \frac{b_{12}}{\hbar}\left[\frac{im_t}{\hbar}E_{\rm VS}(cy_{12}+sx_{12}) + |e|B\cos 2\varphi\,\langle z\rangle\right]\right\}, \tag{B14}$$

$$V_{15} = \left\{ \frac{\alpha_{R;v_1}}{\hbar}\left[\frac{im_t}{\hbar}\Delta_{\rm orb}(cy_{1,m_1} - sx_{1,m_1})\right] + \frac{\beta_{D;v_1}}{\hbar}\left[\frac{im_t}{\hbar}\Delta_{\rm orb}(cx_{1,m_1} - sy_{1,m_1})\right]\right\}, \tag{B15}$$

$$V_{16} = \left\{ -\frac{\alpha_{R;v_1}}{\hbar}\left[\frac{im_t}{\hbar}\Delta_{\rm orb}(cx_{1,m_1} + sy_{1,m_1})\right] - \frac{\beta_{D;v_1}}{\hbar}\left[\frac{im_t}{\hbar}\Delta_{\rm orb}(cy_{1,m_1} + sx_{1,m_1})\right]\right\}. \tag{B16}$$

The remaining matrix elements, $V_{17},\ldots,V_{1,12}$, can be obtained from V_{15}, V_{16} by suitable replacements of the envelopes: $V_{17} = V_{15}(m_1 \to m_2)$, $V_{18} = V_{16}(m_1 \to m_2)$, $V_{19} = V_{15}(m_1 \to \tilde{m}_1, \Delta_{\rm orb} \to \Delta_{\rm orb} + E_{\rm VS})$, $V_{1,10} = V_{16}(m_1 \to \tilde{m}_1, \Delta_{\rm orb} \to \Delta_{\rm orb} + E_{\rm VS})$, $V_{1,11} = V_{19}(m_1 \to \tilde{m}_2)$, and $V_{1,12} = V_{1,10}(m_1 \to \tilde{m}_2)$. For the second series of matrix elements, they are related to the above one (for in-plane magnetic field, $\boldsymbol{B}_\parallel$). Thus $V_{23} = V_{14}$, $V_{24} = -V_{13}$, $V_{25} = V_{16}$, $V_{26} = -V_{15},\ldots,V_{2,12} = -V_{1,11}$.

Using standard second-order perturbation theory for the energy difference $[\delta E_2^{(2)} - \delta E_1^{(2)}]$ and the above relations, one gets

$$\delta E_2^{(2)} - \delta E_1^{(2)} = \frac{2|V_{12}|^2}{E_Z} + |V_{14}|^2\left(\frac{1}{E_Z - E_{\rm VS}} + \frac{1}{E_Z + E_{\rm VS}}\right) + 2|V_{16}|^2\left(\frac{1}{E_Z - \Delta_{\rm orb}} + \frac{1}{E_Z + \Delta_{\rm orb}}\right) + 2|V_{1,10}|^2\left(\frac{1}{E_Z - \Delta_{\rm orb} - E_{\rm VS}} + \frac{1}{E_Z + \Delta_{\rm orb} + E_{\rm VS}}\right), \tag{B17}$$

and for the g-factor one obtains, by grouping the terms

$$\delta E_2^{(2)} - \delta E_1^{(2)} = \delta^{(2)} g_\parallel^{v_1}\ \mu_B B, \quad \delta^{(2)} g_\parallel^{v_1} \equiv \delta g_\parallel^{12} + \delta g_\parallel^{14} + \delta g_\parallel^{16} + \delta g_\parallel^{1,10}. \tag{B18}$$

The relevant contributions read

$$\delta g_\parallel^{12} = \frac{|e|^2}{\hbar^2\mu_B^2}\frac{2}{g^*}\beta_{D;v_1}^2\ \cos^2 2\varphi\,\langle z\rangle^2, \tag{B19}$$

$$\delta g_\parallel^{14} = -\frac{|e|^2}{\hbar^2\mu_B^2}\frac{1}{E_{\rm VS}^2 - E_Z^2}\left\{\frac{2}{g^*}E_Z^2 b_{12}^2\cos^2 2\varphi\,\langle z\rangle^2 + \frac{g^*}{2}E_{\rm VS}^2\frac{m_t^2}{m_0^2}[a_{12}(cx_{12}+sy_{12}) + b_{12}(cy_{12}+sx_{12})]^2\right\}, \tag{B20}$$

$$\delta g_\parallel^{16} + \delta g_\parallel^{18} = -\frac{|e|^2}{\hbar^2\mu_B^2}\frac{g^*}{2}\frac{m_t^2}{m_0^2}\frac{\Delta_{\rm orb}^2}{\Delta_{\rm orb}^2 - E_Z^2}\left\{y_{1,m_1}^2[s\,\alpha_{R;v_1} + c\,\beta_{D;v_1}]^2 + x_{1,m_2}^2[c\,\alpha_{R;v_1} + s\,\beta_{D;v_1}]^2\right\}, \tag{B21}$$

$$\delta g_\parallel^{1,10} + \delta g_\parallel^{1,12} = -\frac{|e|^2}{\hbar^2\mu_B^2}\frac{g^*}{2}\frac{m_t^2}{m_0^2}\frac{(\Delta_{\rm orb} + E_{\rm VS})^2}{(\Delta_{\rm orb} + E_{\rm VS})^2 - E_Z^2}\left\{y_{1,\tilde{m}_1}^2[s\,a_{12} + c\,b_{12}]^2 + x_{1,\tilde{m}_2}^2[c\,a_{12} + s\,b_{12}]^2\right\}. \tag{B22}$$

In the above, we have used (for a circular dot with parabolic confinement) that $x_{1,m_1} = y_{1,m_2} = x_{1,\tilde{m}_1} = y_{1,\tilde{m}_2} = 0$. The standard nonzero dipole matrix elements to orbital states, $y_{1,m_1} = x_{1,m_2} = y_{1,\tilde{m}_1} = x_{1,\tilde{m}_2} = \sqrt{\frac{\hbar^2}{2m_t\Delta_{\rm orb}}}$ will be used for further evaluation of Eqs. (B21) and (B22).

2. Second-order corrections: case of $\boldsymbol{B}_\perp$

For the second-order corrections in perpendicular magnetic field $\boldsymbol{B}_\perp$, we use the SOC Hamiltonian (B5) and include transitions to higher states as was done above. One obtains for the first few matrix elements,

$$V_{12} = \langle\bar{v}_1,\downarrow|\mathcal{H}_{\text{s-v}}|\bar{v}_1,\uparrow\rangle = \hbar^{-1}\langle\phi^{v_1}(\boldsymbol{x})|a_{11}(P_y - iP_x) + b_{11}(P_x - iP_y)|\phi^{v_1}(\boldsymbol{x})\rangle, \tag{B23}$$

$$V_{13} = 0, \tag{B24}$$

$$V_{14} = \langle\bar{v}_1,\downarrow|\mathcal{H}_{\text{s-v}}|\bar{v}_2,\uparrow\rangle = \hbar^{-1}\langle\phi^{v_1}(\boldsymbol{x})|a_{12}(P_y - iP_x) + b_{12}(P_x - iP_y)|\phi^{v_2}(\boldsymbol{x})\rangle, \tag{B25}$$

$$V_{15} = 0, \tag{B26}$$

$$V_{16} = \langle\bar{v}_1,\downarrow|\mathcal{H}_{\text{s-v}}|m_1,\uparrow\rangle = \hbar^{-1}\langle\phi^{v_1}(\boldsymbol{x})|a_{11}(P_y - iP_x) + b_{11}(P_x - iP_y)|\phi^{m_1}(\boldsymbol{x})\rangle, \tag{B27}$$

etc. The structure of the higher matrix elements is similar, e.g., $V_{17} = V_{19} = V_{1,11} = 0$, $V_{18} = V_{16}(m_1 \to m_2)$, $V_{1,10} = V_{16}(m_1 \to \tilde{m}_1)$, $V_{1,12} = V_{16}(m_1 \to \tilde{m}_2)$. For the second series of matrix elements, they are related to the above one (for perpendicular magnetic field, $\boldsymbol{B}_\perp$). Thus $V_{23} = V_{14}(i \to -i)$, $V_{25} = V_{16}(i \to -i)$, $V_{27} = V_{18}(i \to -i)$, $V_{29} = V_{1,10}(i \to -i)$, and $V_{2,11} = V_{1,12}(i \to -i)$. For the squared matrix elements, these replacements correspond to the formal sign change of $E_Z = g^*\mu_B B$ (see below).

Using standard second-order perturbation theory for the energy difference $[\delta E_2^{(2)} - \delta E_1^{(2)}]$ and the above relations, one gets

$$\delta E_2^{(2)} - \delta E_1^{(2)} = \frac{2|V_{12}|^2}{E_Z} + \left(\frac{|V_{23}|^2}{E_Z - E_{\rm VS}} + \frac{|V_{14}|^2}{E_Z + E_{\rm VS}}\right) + \left(\frac{|V_{25}|^2}{E_Z - \Delta_{\rm orb}} + \frac{|V_{16}|^2}{E_Z + \Delta_{\rm orb}}\right) + (m_1 \to m_2) + \left(\frac{|V_{29}|^2}{E_Z - \Delta_{\rm orb} - E_{\rm VS}} + \frac{|V_{1,10}|^2}{E_Z + \Delta_{\rm orb} + E_{\rm VS}}\right) + (\tilde{m}_1 \to \tilde{m}_2). \tag{B28}$$

The matrix elements V_{ab}, $a = 1, 2$, $b = 1, \ldots, 12$, are calculated similar to the previous case, using the equation of motion, Eq. (B11).

Having at hand these matrix elements, we use the second-order correction to the energy difference, Eq. (B28), and group the terms accordingly:

$$\delta E_2^{(2)} - \delta E_1^{(2)} = \delta^{(2)} g_\perp^{v_1}\, \mu_B B, \quad \delta^{(2)} g_\perp^{v_1} \equiv \delta g_\perp^{12} + \delta g_\perp^{14} + \delta g_\perp^{16} + \delta g_\perp^{18} + \delta g_\perp^{1,10} + \delta g_\perp^{1,12}. \tag{B29}$$

The relevant contributions to $\delta^{(2)} g_\perp$ read

$$\delta g_\perp^{12} = \frac{|e|^2}{\hbar^2 \mu_B^2} \frac{1}{2g^*} \{(x_{11}\alpha_{R;v_1} - y_{11}\beta_{D;v_1})^2 + (x_{11}\beta_{D;v_1} - y_{11}\alpha_{R;v_1})^2\}, \tag{B30}$$

which coincides with Eq. (63), as expected. Also,

$$\delta g_\perp^{14} = \frac{g^*}{E_Z}\left[\frac{|V_{14}|^2}{E_Z + E_{\rm VS}} + \frac{|V_{23}|^2}{E_Z - E_{\rm VS}}\right] = \frac{|e|^2}{4\hbar^2\mu_B^2} \frac{1}{h_z\left(\frac{m_0}{m_t} + 2h_z\right)} \{[x_{12}\, a_{12}(1 - h_z) + y_{12}\, b_{12}(1 + h_z)]^2 + [x_{12}\, b_{12}(1 + h_z) + y_{12}\, a_{12}(1 - h_z)]^2\} + (h_z \to -h_z) \tag{B31}$$

with $h_z \equiv \frac{m_0}{m_t}\frac{E_Z}{2E_{\rm VS}}$.

$$\delta g_\perp^{16} + \delta g_\perp^{18} = \frac{g^*}{E_Z}\left[\frac{|V_{16}|^2}{E_Z + \Delta_{\rm orb}} + \frac{|V_{25}|^2}{E_Z - \Delta_{\rm orb}}\right] + (m_1 \to m_2) = \frac{|e|^2}{4\hbar^2\mu_B^2} \frac{1}{\tilde{h}_z\left(\frac{m_0}{m_t} + 2\tilde{h}_z\right)} \left\{\left(y_{1,m_1}^2 + x_{1,m_2}^2\right)\left(\alpha_{R;v_1}^2(1 - \tilde{h}_z)^2 + \beta_{D;v_1}^2(1 + \tilde{h}_z)^2\right)\right\} + (\tilde{h}_z \to -\tilde{h}_z) \tag{B32}$$

with $\tilde{h}_z \equiv \frac{m_0}{m_t}\frac{E_Z}{2\Delta_{\rm orb}}$.

$$\delta g_\perp^{1,10} + \delta g_\perp^{1,12} = \frac{g^*}{E_Z}\left[\frac{|V_{1,10}|^2}{E_Z + \Delta_{\rm orb} + E_{\rm VS}} + \frac{|V_{29}|^2}{E_Z - \Delta_{\rm orb} - E_{\rm VS}}\right] + (\tilde{m}_1 \to \tilde{m}_2) = \frac{|e|^2}{4\hbar^2\mu_B^2} \frac{1}{\bar{h}_z\left(\frac{m_0}{m_t} + 2\bar{h}_z\right)} \left\{\left(y_{1,\tilde{m}_1}^2 + x_{1,\tilde{m}_2}^2\right)\left(a_{12}^2(1 - \bar{h}_z)^2 + b_{12}^2(1 + \bar{h}_z)^2\right)\right\} + (\bar{h}_z \to -\bar{h}_z) \tag{B33}$$

with $\bar{h}_z \equiv \frac{m_0}{m_t}\frac{E_Z}{2(\Delta_{\rm orb} + E_{\rm VS})}$. In the above, we have used the relations for the dipole matrix elements to orbital states, see text after Eqs. (B21) and (B22).

As mentioned above, for an interface with roughness, the lowest energy envelopes, $\phi^{v_i}(x, y)$ (quasi-s-like), acquire a p-like contribution, depending on the eigenvalley index v_i. Thus the dipole matrix elements $\boldsymbol{r}_{ij} \equiv \langle v_i|\boldsymbol{r}|v_j\rangle$ $i, j = 1, 2$ are generally nonzero [7,40], getting a size of few nanometers for this type of QDs [7].

3. δg at the spin-valley anticrossing point

At the anticrossing (at the so-called "relaxation hot spot") [7], when $E_Z \approx E_{\rm VS}$, the contribution $\delta g_\parallel^{14}$ acquires a first-order correction (by solving the standard secular equation). The exact qubit energy difference is $\frac{1}{2}[E_{\rm VS} + E_Z - \sqrt{(E_{\rm VS} - E_Z)^2 + \Delta_a^2}]$, where

$$\Delta_a = 2|V_{23}| = 2|V_{14}| \tag{B34}$$

is the splitting at anticrossing of the relevant valley states [7,8] $|2\rangle$ and $|3\rangle$, see Eqs. (B14), (B25), and Fig. 1(d). Close to anticrossing, when $\delta \equiv E_{\rm VS} - E_Z \lesssim \Delta_a$,

$$\delta g_{\text{hot-spot}} = -\frac{\Delta_a}{E_Z} + \frac{\delta}{E_Z} - \frac{\delta^2}{2\Delta_a E_Z}. \tag{B35}$$

Thus $\delta g_{\text{hot-spot}}$ may be of the order of 10^{-3} or less since the splitting was evaluated [7,8] as $\Delta_a = (10^{-3}$–$10^{-4})\, E_{\rm VS}$. This is at least 10 times smaller than the observed experimental g-factor correction [11,13], as presented in Fig. 3. Also, there is no observed deviation from the linear dependence with F_z near the anticrossing point which restricts the size of Δ_a.

4. The integral relation, Eq. (24), for a z-confinement potential $U(z)$ with an infinite boundary

One starts with the one-dimensional eigenvalue problem

$$-\frac{\hbar^2}{2m}\varphi''(z)+U(z)\varphi(z)-E\varphi(z)=0 \tag{B36}$$

with $\varphi(0)=0$. By multiplying Eq. (B36) by $\varphi^{*\prime}(z)$ and integrating by parts the first and last term,

$$\int_0^\infty dz\varphi^{*'}(z)\varphi''(z)=-\varphi^{*\prime}(0)\varphi'(0)-\int_0^\infty dz\varphi^{*\prime\prime}(z)\varphi'(z) \tag{B37}$$

$$-E\int_0^\infty dz\varphi^{*\prime}(z)\varphi(z)=E\int_0^\infty dz\varphi^{*}(z)\varphi'(z), \tag{B38}$$

then one adds the conjugate 1D equation, multiplied by $\varphi'(z)$. As a result, $-\int_0^\infty dz\frac{2m}{\hbar^2}U(z)\frac{d}{dz}|\varphi(z)|^2=|\varphi'(0)|^2$ or

$$\frac{2m}{\hbar^2}\int_0^\infty dz\varphi^*(z)\partial_z U(z)\varphi(z)=|\varphi'(0)|^2. \tag{B39}$$

APPENDIX C: INTERFACE BOUNDARY CONDITION FROM HERMITICITY OF THE HAMILTONIAN

1. Volkov-Pinsker boundary condition

For completeness, we first rederive the Volkov-Pinsker BC [34], starting from the single-band approximation Hamiltonian, in the presence of an external field, $\boldsymbol{A}(\boldsymbol{r})$:

$$\mathcal{H}=\frac{(\boldsymbol{p}+|e|\boldsymbol{A})^2}{2m}+U(\boldsymbol{r}). \tag{C1}$$

Considering two arbitrary solutions, ϕ_1,ϕ_2 of the Schrödinger equation, one states the hermiticity condition at the half-space, $z>z_0$ [34]:

$$\int_{z>z_0}dz\,\phi_1^\dagger(\mathcal{H}\phi_2)=\int_{z>z_0}dz\,\phi_2(\mathcal{H}\phi_1)^*. \tag{C2}$$

Substituting $\mathcal{H}$ in Eq. (C2), and integrating by parts one gets the relation (put $\hbar=e=1$)

$$\phi_2(z_0)\frac{d\phi_1^*}{dz}-\phi_1^*(z_0)\frac{d\phi_2}{dz}+2i\phi_1^*(z_0)A_z(z_0)\phi_2(z_0)=0, \tag{C3}$$

where separation of variables is assumed for the potential, Eq. (14). Equation (C3) can be satisfied if

$$\frac{1}{\phi_1}\frac{d\phi_1(z_0)}{dz}=\frac{1}{\phi_2}\frac{d\phi_2(z_0)}{dz}=\text{const.}+iA_z(z_0). \tag{C4}$$

By choosing const $\equiv-\frac{1}{R}$, one can recast Eq. (C4) to the BC:

$$\left\{1+i\frac{R}{\hbar}(p_z+|e|A_z)\right\}\phi(z)\,|_{z_0^+}=0, \tag{C5}$$

with $p_z\equiv-i\hbar\partial_z$. For $A_z=0$ one recovers Eq. (8). As follows from Eq. (C5), the gauge invariance of the Schrodinger equation plus boundary conditions implies in general "extension of derivatives" both in the Hamiltonian and in the boundary conditions. In case of the spin-valley BCs considered in the main text, Eqs. (6), (15), and (43), one should extent both the ∂_z derivative as well as the $\partial_{x,y}$ derivatives.

Notice also that the bulk velocity operator is $v_z\equiv\frac{\partial\mathcal{H}}{\partial p_z}=\frac{1}{m}(p_z+|e|A_z)$. The hermiticity condition, Eq. (C3), then can be rewritten as

$$\phi_1^*(v_z\phi_2)+(v_z\phi_1)^*\phi_2\;|_{z_0^+}=0. \tag{C6}$$

This implies continuity of the envelope flux density, despite of the discontinuity of the wave function at its derivative at the interface.

2. BC and gauge invariance

Concerning the gauge invariance, we have already mentioned in Sec. IV A that the problem (Hamiltonian plus boundary conditions) is written in a gauge invariant form, via the extension of the derivatives. Therefore, in the actual calculations, one is using the most convenient gauge as is, e.g., with the results for the g-factor renormalization, Eqs. (45)–(55). One may ask the question how the gauge invariance is preserved during the derivation, e.g., of Eq. (55)? We mention that any gauge change leads to a multiplication of the wave function with a phase factor, which cancels in the quantum average $\langle z\rangle$ in Eq. (55) [considering a boundary at $z_0=0$]. By using the gauge $\boldsymbol{A}_\parallel(\boldsymbol{r})=(z,-z,0)B/\sqrt{2}$, for each of the two spin components, there is a modification of the z-confinement potential of Eq. (14) by a linear z term. This leads to a modification of the eigenvalues of the original problem, Eq. (12), which ends up with the result (55) as a first-order correction. Since we are considering a homogeneous magnetic field, the vector potential is a linear function of the coordinates, including also an arbitrary constant vector. For example, for the gauge $\boldsymbol{A}'=\boldsymbol{A}_\parallel(\boldsymbol{r})+(c,-c,0)$, one naively would expect a shift in the z coordinate. This gauge transformation, however, corresponds to adding a constant to the Hamiltonian (12), which does not change the eigenvalues. Thus the gauge invariance is preserved in this case.

One may consider the gauge $\boldsymbol{A}''=(0,0,y-x)B/\sqrt{2}$, which is more involved. Indeed, in this case, there is no explicit z, and it is puzzling how one can obtain the $\langle z\rangle$ in the final result. One starts with the BC, Eq. (6), in the form

$$\left\{1+iR\left(k_z+\frac{|e|}{\hbar}A_z\right)-R\,\frac{2m_l}{\hbar^2}\,V_{\rm if}(\boldsymbol{k})\right\}\Phi(\boldsymbol{r})\,|_{z=0^+}$$
$$\equiv\mathcal{B}(A_z)\Phi(\boldsymbol{r})\,|_{z=0^+}=0, \tag{C7}$$

and following the derivations of Eqs. (17) and (18), one obtains the effective unitary transform (see Appendix A)

$$\Gamma_{\rm BC}(A_z)=1+i\left[R\left(k_z+\frac{|e|}{\hbar}A_z\right)\right.$$
$$\left.+R^2\frac{2m_l}{\hbar^2}V_{\rm if}(\boldsymbol{k})\left(k_z+\frac{|e|}{\hbar}A_z\right)\right] \tag{C8}$$

such that $\Gamma_{\rm BC}(A_z)\Phi(\boldsymbol{r})\,|_{z=0^+}\simeq 0$. After some elaborate calculations, using the above described procedure, one can obtain a term in the effective Hamiltonian perturbation, ΔH, which is k_z^2. Thus, since $\langle k_z^2\rangle=\text{const}\,\langle z\rangle$ for the triangular potential in Eq. (12), $\langle z\rangle$ is recovered.

3. Estimation of the *R* parameter

One can illustrate how an effective length parameter R appears in a single-band BC like Eq. (C5) from a two-band model [34], with two-component envelope, $\phi^T = [\phi_c(\boldsymbol{r}), \phi_v(\boldsymbol{r})]$, including conduction and valence bands. Neglecting $\mathcal{O}(p_z^2)$ effects, the $\boldsymbol{k}\cdot\boldsymbol{p}$-Hamiltonian is

$$\mathcal{H}^{2\text{band}} = \begin{pmatrix} E_c & \frac{p_{cv}}{m_0} p_z \\ \frac{p_{cv}^*}{m_0} p_z & E_v \end{pmatrix}, \tag{C9}$$

where p_{cv} is the interband momentum matrix element. The BC, Eq. (C6), is recast to $(-\phi_{1v}^* \phi_{2c} + \phi_{1c}^* \phi_{2v})\,|_{z_0^+} = 0$, for any two functions, ϕ_1, ϕ_2. On the other hand, a stationary solution of the Schrödinger equation with $\mathcal{H}^{2\text{band}}$ gives a relation: $\phi_c = -\frac{p_{cv} p_z}{(E_c - E) m_0}\phi_v$ (and analogous one, with $c \to v$), allowing to exclude the other band. [It is worth to stress here that such relations make it impossible to have simultaneously $\phi_c(z_0) = 0$ and $\phi_v(z_0) = 0$, as required by the standard BC with infinite boundary.] Compatibility of the two-band BC with the single-band BC, Eq. (C5), leads to the relation [34] $R_c \simeq R_v = \frac{1}{2}\sqrt{\frac{2\hbar^2}{m_c^* E_{\text{gap}}}}$, where $E_{\text{gap}} = E_c - E_v \approx 4\,\text{eV}$ is the band gap in Si at the band minima, m_c^* is the effective mass, and we have used the approximate relation [73] $\frac{m_0}{m_c^*} \approx \frac{2p_{cv}^2}{m_0 E_{\text{gap}}}$. Thus, as a rough estimation (i.e., not taking into account valleys), one gets $R = R_c^{\text{Si}} \approx 0.1$–$0.2$ nm for $m_t < m_c^* < m_l$.

[1] E. I. Rashba and V. I. Sheka, *Electric-Dipole Spin Resonances In: Landau Level Spectroscopy*, edited by G. Landwehr and E. I. Rashba (Elsevier Science, Amsterdam, 1991).
[2] S. Datta and B. Das, Appl. Phys. Lett. **56**, 665 (1990).
[3] M. Hasan and C. Kane, Rev. Mod. Phys. **82**, 3045 (2010).
[4] R. Jansen, Nat. Mater. **11**, 400 (2012).
[5] F. Zwanenburg, A. S. Dzurak, A. Morello, M. Y. Simmons, L. C. L. Hollenberg, G. Klimeck, S. Rogge, S. N. Coppersmith, and M. A. Eriksson, Rev. Mod. Phys. **85**, 961 (2013).
[6] B. M. Maune, M. G. Borselli, B. Huang, T. D. Ladd, P. W. Deelman, K. S. Holabird, A. A. Kiselev, I. Alvarado-Rodriguez, R. S. Ross, A. E. Schmitz, M. Sokolich, C. A. Watson, M. F. Gyure, and A. T. Hunter, Nature (London) **481**, 344 (2012).
[7] C. H. Yang, A. Rossi, R. Ruskov, N. S. Lai, F. A. Mohiyaddin, S. Lee, C. Tahan, G. Klimeck, A. Morello, and A. S. Dzurak, Nat. Commun. **4**, 2069 (2013).
[8] X. Hao, R. Ruskov, M. Xiao, C. Tahan, and H. Jiang, Nat. Commun. **5**, 3860 (2014).
[9] D. Kim, Z. Shi, C. B. Simmons, D. R. Ward, J. R. Prance, T. S. Koh, J. K. Gamble, D. E. Savage, M. G. Lagally, M. Friesen, S. N. Coppersmith, and M. A. Eriksson, Nature (London) **511**, 70 (2014).
[10] E. E. Kawakami, P. Scarlino, D. R. Ward, F. R. Braakman, D. E. Savage, M. G. Lagally, M. Friesen, S. N. Coppersmith, M. A. Eriksson, and L. M. K. Vandersypen, Nat. Nanotechnol. **9**, 666 (2014).
[11] M. Veldhorst, J. C. C. Hwang, C. H. Yang, A. W. Leenstra, B. de Ronde, J. P. Dehollain, J. T. Muhonen, F. E. Hudson, K. M. Itoh, A. Morello, and A. S. Dzurak, Nat. Nanotechnol. **9**, 981 (2014).
[12] M. Veldhorst, C. H. Yang, J. C. C. Hwang, W. Huang, J. Dehollain, J. Muhonen, S. Simmons, A. Laucht, F. Hudson, K. Itoh, A. Morello, and A. Dzurak, Nature (London) **526**, 410 (2015).
[13] M. Veldhorst, R. Ruskov, C. H. Yang, J. C. C. Hwang, F. E. Hudson, M. E. Flatté, C. Tahan, K. M. Itoh, A. Morello, and A. S. Dzurak, Phys. Rev. B **92**, 201401(R) (2015).
[14] R. Ferdous, E. Kawakami, P. Scarlino, M. P. Nowak, D. R. Ward, D. E. Savage, M. G. Lagally, S. N. Coppersmith, M. Friesen, M. A. Eriksson, L. M. K. Vandersypen, and R. Rahman, NPJ Quantum Inf. **4**, 26 (2018).
[15] R. Ferdous, K. W. Chan, M. Veldhorst, J. C. C. Hwang, C. H. Yang, H. Sahasrabudhe, G. Klimeck, A. Morello, A. S. Dzurak, and R. Rahman, Phys. Rev. B **97**, 241401(R) (2018).
[16] R. M. Jock, N. T. Jacobson, P. Harvey-Collard, A. M. Mounce, V. Srinivasa, D. R. Ward, J. Anderson, R. Manginell, J. R. Wendt, M. Rudolph, T. Pluym, J. K. Gamble, A. D. Baczewski, W. M. Witzel, and M. S. Carroll, Nat. Commun. **9**, 1768 (2018).
[17] A. Corna, L. Bourdet, R. Maurand, A. Crippa, D. Kotekar-Patil, H. Bohuslavskyi, R. Lavieville, L. Hutin, S. Barraud, X. Jehl, M. Vinet, S. De Franceschi, Y.-M. Niquet, and M. Sanquer, NPJ Quantum Inf. **4**, 6 (2018).
[18] T. Tanttu, B. Hensen, K. W. Chan, H. Yang, W. Huang, M. Fogarty, F. Hudson, K. Itoh, D. Culcer, A. Laucht, A. Morello, and A. Dzurak, Controlling spin-orbit interactions in silicon quantum dots using magnetic field direction, arXiv:1807.10415v3 [cond-mat].
[19] K. M. Itoh and H. Watanabe, MRS Commun. **4**, 143 (2014).
[20] L. M. Roth, Phys. Rev. **118**, 1534 (1960).
[21] L. Liu, Phys. Rev. **126**, 1317 (1962).
[22] F. J. Ohkawa and Y. Uemura, J. Phys. Soc. Jpn. **43**, 907 (1977).
[23] L. J. Sham and M. Nakayama, Phys. Rev. B **20**, 734 (1979).
[24] M. Friesen, S. Chutia, C. Tahan, and S. N. Coppersmith, Phys. Rev. B **75**, 115318 (2007).
[25] M. O. Nestoklon, E. L. Ivchenko, J.-M. Jancu, and P. Voisin, Phys. Rev. B **77**, 155328 (2008).
[26] A. L. Saraiva, M. J. Calderón, X. Hu, S. Das Sarma, and B. Koiller, Phys. Rev. B **80**, 081305(R) (2009).
[27] E. L. Ivchenko and A. A. Kiselev, Sov. Phys. Semiconductors-USSR **26**, 827 (1992).
[28] A. A. Kiselev, E. L. Ivchenko, and U. Rössler, Phys. Rev. B **58**, 16353 (1998).
[29] F. T. Vasko and N. A. Prima, Fiz. Tverdogo Tela **23**, 2042 (1981).
[30] A. V. Rodina, A. L. Efros, and A. Y. Alekseev, Phys. Rev. B **67**, 155312 (2003).
[31] A. V. Rodina and A. Y. Alekseev, Phys. Rev. B **73**, 115312 (2006).
[32] A. A. Kiselev, E. L. Ivchenko, and M. Willander, Solid State Commun. **102**, 375 (1997).
[33] J.-M. Jancu, R. Scholz, E. A. de Andrada e Silva, and G. C. La Rocca, Phys. Rev. B **72**, 193201 (2005).
[34] V. A. Volkov and T. N. Pinsker, Surface Science **81**, 181 (1979).

[35] F. T. Vasko and A. V. Kuznetsov, *Electronic States and Optical Transitions in Semiconductor Heterostructures* (Springer, New York, 1998).

[36] T. Ando and S. Mori, Sur. Sci. **113**, 124 (1982).

[37] I. V. Tokatly, A. G. Tsibizov, and A. A. Gorbatsevich, Phys. Rev. B **65**, 165328 (2002).

[38] L. S. Braginsky, Phys. Rev. B **60**, R13970 (1999).

[39] Z. A. Devizorova and V. A. Volkov, JETP Letters **100**, 102 (2014).

[40] J. K. Gamble, M. A. Eriksson, S. N. Coppersmith, and M. Friesen, Phys. Rev. B **88**, 035310 (2013).

[41] F. J. Ohkawa and Y. Uemura, J. Phys. Soc. Jpn. **43**, 917 (1977).

[42] F. J. Ohkawa, Solid State Commun. **26**, 69 (1978).

[43] T. B. Boykin, G. Klimeck, M. Friesen, S. N. Coppersmith, P. von Allmen, F. Oyafuso, and S. Lee, Phys. Rev. B **70**, 165325 (2004).

[44] M. O. Nestoklon, L. E. Golub, and E. L. Ivchenko, Phys. Rev. B **73**, 235334 (2006).

[45] L. E. Golub and E. L. Ivchenko, Phys. Rev. B **69**, 115333 (2004).

[46] W. Kohn and J. M. Luttinger, Phys. Rev. **98**, 915 (1955).

[47] F. T. Vasko, JETP Lett. **30**, 541 (1979).

[48] L. S. Braginsky, Phys. Rev. B **57**, R6870 (1998).

[49] I. E. Tamm, Phys. Z. Sowjetunion **1**, 733 (1932).

[50] D. Culcer, X. Hu, and S. Das Sarma, Phys. Rev. B **82**, 205315 (2010).

[51] M. Friesen and S. N. Coppersmith, Phys. Rev. B **81**, 115324 (2010).

[52] For a Si/SiO_2 interface, with a valley splitting [7] $E_{VS} \approx 300\mu$eV–800μeV, and estimated SOC couplings, Eqs. (69) and (70), one gets $E_{VS} \gg |\beta_{D;v_i}| \langle k_{x,y} \rangle \approx 30 - 50\mu$eV, with $\langle k_{x,y} \rangle \sim 1/l_D = (\hbar/m_t\omega_0)^{-1/2} \approx 10^6\,\mathrm{cm}^{-1}$.

[53] Using the tight-binding result [24] for the valley splitting parameter, $|V| \simeq 720\,\Delta_{\mathrm{offset}}$, one gets $|V|_{Si/SiO_2} = 2160$ meV Å at $\Delta_{\mathrm{offset}} = 3$eV for a Si/SiO_2 interface.

[54] For arbitrary interface position z_0, the z_0 dependence cancels in the phase differences, $\phi_R(z_0) - \phi_V(z_0) = \phi_R - \phi_V$, $\phi_D(z_0) - \phi_V(z_0) = \phi_D - \phi_V$, as required by translational invariance.

[55] These BCs, Eq. (43), are similar to that derived for single-valley heterostructures with an abrupt interface [31,39].

[56] D. Wilson and G. Feher, Bull. Am. Phys. Soc. **5**, 60 (1960).

[57] R. Ruskov, Invited talk at the Silicon quantum electronics conference, Delft, The Netherlands, June 13-14, (2016).

[58] C. Tahan, Talk at the Quantum Computing Program Review, San Diego, CA, Aug 10-12, (2015).

[59] R. Ferdous and R. Rahman (private communication).

[60] E. Magesan, J. M. Gambetta, B. R. Johnson, C. A. Ryan, J. M. Chow, S. T. Merkel, M. P. da Silva, G. A. Keefe, M. B. Rothwell, T. A. Ohki, M. B. Ketchen, and M. Steffen, Phys. Rev. Lett. **109**, 080505 (2012).

[61] M. A. Fogarty, M. Veldhorst, R. Harper, C. H. Yang, S. D. Bartlett, S. T. Flammia, and A. S. Dzurak, Phys. Rev. A **92**, 022326 (2015).

[62] A. N. Korotkov, Phys. Rev. B **67**, 235408 (2003).

[63] C. Tahan, M. Friesen, and R. Joynt, Phys. Rev. B **66**, 035314 (2002).

[64] S. Goswami, K. A. Slinker, M. Friesen, L. M. McGuire, J. L. Truitt, C. Tahan, L. J. Klein, J. O. Chu, P. M. Mooney, D. W. van Derweide, R. Joynt, S. N. Coppersmith, and M. A. Eriksson, Nat. Phys. **3**, 41 (2007).

[65] N. Shaji, C. B. Simmons, M. Thalakulam, L. J. Klein, H. Qin, H. Luo, D. E. Savage, M. G. Lagally, A. J. Rimberg, R. Joynt, M. Friesen, R. H. Blick, S. N. Coppersmith, and M. A. Eriksson, Nat. Phys. **4**, 540 (2008).

[66] D. Culcer, L. Cywiński, Q. Li, X. Hu, and S. Das Sarma, Phys. Rev. B **82**, 155312 (2010).

[67] M. J. Rančić and G. Burkard, Phys. Rev. B **93**, 205433 (2016).

[68] E. Prati, Jn Nanosci. Nanotechnol. **11**, 8522 (2011).

[69] D. Culcer, A. L. Saraiva, B. Koiller, X. Hu, and S. Das Sarma, Phys. Rev. Lett. **108**, 126804 (2012).

[70] J. Levy, Phys. Rev. Lett. **89**, 147902 (2002).

[71] Y.-P. Shim and C. Tahan, Phys. Rev. B **93**, 121410(R) (2016).

[72] M. A. Bakker, S. Mehl, T. Hiltunen, A. Harju, and D. P. DiVincenzo, Phys. Rev. B **91**, 155425 (2015).

[73] P. Yu and M. Cardona, *Fundamentals of Semiconductors* (Springer, Berlin, 2010).